

Article

Numerical Study on Effects of Geometric Parameters on the Release Characteristics of Straight Sudden Expansion Gas Extinguishing Nozzles

Quanwei Li ^{1,*} , Xiaohua He ², Yongbing Chen ², Jiang Lin ^{1,3}, Yi Zhang ¹, Ruiyu Chen ¹  and Xia Zhou ¹

¹ School of Chemistry and Chemical Engineering, Nanjing University of Science and Technology, Nanjing 210094, China; salutino@njjust.edu.cn (J.L.); zhangyi0911@njjust.edu.cn (Y.Z.); crynjust@njjust.edu.cn (R.C.); zhoxia@njjust.edu.cn (X.Z.)

² Shanghai Space Propulsion Technology Research Institute, Huzhou 313000, China; nancy.he@fairtech.com.cn (X.H.); chen Yongbin@njau.edu.cn (Y.C.)

³ COMAC Shanghai Aircraft Manufacturing Co., Ltd., Shanghai 201302, China

* Correspondence: liqw@njjust.edu.cn; Tel.: +86-025-8430-3159

Abstract: In order to guide the optimization design of the nozzle of the aircraft-fixed gas fire extinguishing system, we studied the influence of nozzle geometric parameters including outlet–inlet area ratio, length–diameter aspect ratio, and wall roughness on the distribution of pressure and velocity in the nozzle on the basis of CFD simulations. Although the structure of the nozzle is axisymmetric, the spatial distribution of the pressure and velocity during the flow and release of gas extinguishing agent is not completely symmetric. It was found that both of the outlet–inlet area ratio (δ) and the length–diameter aspect ratio (ξ) had a significant impact on the distribution characteristics of the pressure and axial velocity in the nozzle. With the increase of δ , the average pressure at the outlet cross-section of the nozzle decreased monotonically, while the average axial velocity at the outlet increased approximately linearly. When $\xi \geq 2$, the uniformity of the pressure and velocity distribution at the nozzle outlet was significantly improved. Moreover, with the increase of ξ , the average pressure and the average axial velocity of the outlet both showed a non-monotonic change trend, and the optimal value of ξ should be about 3.0. Compared with δ and ξ , the influence of the nozzle wall roughness (ε_N) on the flow and release characteristics of the extinguishing agent was weak. With the increase of ε_N , the average pressure of the nozzle outlet increased slightly, while the average axial velocity at the nozzle outlet decreased slightly.

Keywords: aircraft fire extinguishing system; straight sudden expansion nozzle; gas–liquid two-phase flow; gas extinguishing agent; pressure and velocity distribution



Citation: Li, Q.; He, X.; Chen, Y.; Lin, J.; Zhang, Y.; Chen, R.; Zhou, X. Numerical Study on Effects of Geometric Parameters on the Release Characteristics of Straight Sudden Expansion Gas Extinguishing Nozzles. *Symmetry* **2021**, *13*, 2440. <https://doi.org/10.3390/sym13122440>

Academic Editors: Qiang Wang, Xiaolei Zhang, Wei Tang, Jianping Zhang and Xiaochun Zhang

Received: 31 October 2021

Accepted: 10 December 2021

Published: 17 December 2021

Publisher's Note: MDPI stays neutral with regard to jurisdictional claims in published maps and institutional affiliations.



Copyright: © 2021 by the authors. Licensee MDPI, Basel, Switzerland. This article is an open access article distributed under the terms and conditions of the Creative Commons Attribution (CC BY) license (<https://creativecommons.org/licenses/by/4.0/>).

1. Introduction

Fire extinguishing system is one of the essential important security systems on modern aircrafts [1]. Due to the particularity of the aircraft as an important air traffic tool, extremely high requirements for both reliability and economy are put forward for the performance of its fire extinguishing system [2–5]. As an important component of fire extinguishing systems, nozzles usually have a vital impact on the flow and release characteristics of the extinguishing agent, and their release performance has become one of the hot spots of the fire extinguishing technology research in recent years [6–14]. Studies have shown that even if the nozzle structure is axisymmetric, the flow field inside it will be asymmetrically distributed [14]. In fact, the flow and release performance of the nozzle is significantly affected by the nozzle geometric parameters [15–18]. Reasonable design of the extinguishing nozzle can greatly improve the fire extinguishing performance of fire extinguishing systems. Therefore, studying the effects of the nozzle geometric parameters on the flow and release characteristics of the extinguishing agent in the nozzle has a particularly important

applicable value and can provide effective theoretical guidance for the nozzle optimization design of the aircraft fire extinguishing system.

There are many different types of nozzles that are widely used in many fields such as spray cooling, splash lubrication, steam jet, and fire protection. The structure of these nozzles are particularly different, and the commonly used structures are orifice nozzles (generally employed in spray-related fields), Laval nozzles (usually used in applications related to supersonic injection), straight expansion/contraction nozzles (commonly used in the field of gas extinguishing agent injection), etc. In recent years, many numerical simulation studies have been carried out, focusing on the improvement of the flow and release performance of nozzles [6–9,11–13,15–28].

As for orifice nozzles, studies have mainly focused on the improvement of spray characteristics, such as droplet size, droplet velocity, spray cone angle, and shape, of single-phase liquids such as water, oil, and solution [6,7,9,11,12,22]. For example, Lee et al. [16,24,25] studied the influence of the orifice length and orifice diameter of the plain orifice nozzle on the spray characteristics of high-temperature hydrocarbon liquid fuel by combining numerical simulation with an experiment. They found that for injectors of the same orifice diameter, the discharge coefficient decreases with the increase of the orifice length, while for injectors of the same orifice length, the discharge coefficient does not change with the orifice diameter. On the basis of the large eddy numerical simulation method, Zhang et al. [19] studied the influence of nozzle structure on the diffusion angle and volume flux characteristics of the jet oil sprayed by nozzles of gear cases. They found that the jet diffusion angle was approximately zero in the region near the nozzle outlet when the length-diameter aspect ratio was greater than 2, and the change of the orifice diameter and orifice length will change the local loss and the linear loss of the flow, which will finally lead to variation of volume flux of the jet.

As for Laval nozzles, there are many studies focused on the influence of geometric parameters, such as distance ratio, throat diameter, and area ratio, on the performance of base pressure control, steam ejection, and spray forming [8,15,17,18,20,23,26,27]. For example, on the basis of the computational fluid dynamic (CFD) method, Pathan et al. [8] studied the influence of the Laval nozzle pressure ratio on the base pressure for the compressed air under the conditions of constant nozzle length–diameter aspect ratio and area ratio. They found that the higher nozzle pressure ratio had an obvious beneficial effect on the increase of the base pressure when the jets released from the nozzles were under-expanded.

As for straight expansion/contraction nozzles, scarce attention has been paid to the numerical simulation of the flow and release characteristics of them in recent years. Since abrupt flow area expansion is a common phenomenon in various industrial applications, some published studies have focused on the problem of sudden expansion in the flow area in pipes, and some of them are numerical simulation studies for gas–liquid two-phase flow. For example, on the basis of the solving of the one-dimensional conservation equations, Attou et al. [29] compared the predictions of the homogeneous flow model, frozen flow model, and bubbly flow model with experimental results, developing a semi-analytical model for the pressure drop of air–water two-phase flow in sudden enlargements. Roul et al. [30] also explored the pressure drop caused by the sudden expansion/contraction of the flow area in the small round pipes by employing two-phase flow models in an Eulerian scheme. They found that the simulation results of the pressure changes of the air and water mixtures two-phase flow, which was caused by the sudden expansion and contraction of the flow area, were in good agreement with those predicted by the slip flow model. It can be found that there are many relative simulation studies on sudden expansion of pipes, focusing on the pressure loss characteristics during the flow. Furthermore, due to the fact that the boiling point and gasification latent heat of the gas extinguishing agent are significantly different from those of common research objects similar to water (the boiling points of Halon 1301 gas extinguishing agent and water are $-57.8\text{ }^{\circ}\text{C}$ and $100\text{ }^{\circ}\text{C}$, respectively; and the latent heat of vaporization of them are 117.0 kJ/kg and 2257.2 kJ/kg , respectively), the gasification rate of the gas extinguishing

agent is significantly different from that of common liquid mediums. Moreover, since the flow in the aforementioned studies is completely in the tube, the obvious difference from nozzle injection is that there is no influence of the external atmosphere on the flow and phase transformation of the mixture. In fact, as Etzold et al. [6] found that by comparing the numerical simulation results of short nozzles with the experimental data, the properties of the ambient gas boundary layer around the liquid jets had a significant influence on the discrepancies between simulation results and experimental data. Therefore, considering that there is a violent gasification phase transition during the process of gas extinguishing agent releasing from the nozzle into the atmosphere, and the straight sudden expansion nozzle, as a typical representative of straight expansion/contraction nozzles, are commonly used in aircraft fixed gas fire extinguishing systems due to its simple structure, high reliability, and good consistency, it is of great practical value to carry out the research on the flow and release characteristics of straight sudden expansion gas extinguishing nozzles.

It is noteworthy that the geometric parameters, such as outlet–inlet area ratio, length–diameter aspect ratio, and wall roughness, have a significant influence on the distribution of pressure and velocity characteristics during the release process of the gas extinguishing nozzles. However, the influence has drawn little attention in previous studies. Moreover, it is a considerably complex gas–liquid two-phase flow that the fire extinguishing agent flows in the sudden expansion nozzles. This process is accompanied with a significant phase transition. The distribution characteristics of both of the pressure and velocity in the nozzle are extremely important, but these characteristics are much more difficult to be accurately quantitatively characterized by experiments. However, numerical simulation can successfully address this deficiency.

Therefore, in order to deeply understand the flow and release characteristics and internal mechanisms of the fire-extinguishing agent released from the straight sudden expansion nozzle, we established a simplified simulation model for the straight sudden expansion nozzle of the gas fire extinguishing agent in this work, which can guide the optimization design of the aircraft gas fire extinguishing system to promote its performance. On the basis of this model, we analyzed the spatial distribution characteristics of pressure and velocity in the nozzle. The influence of the outlet–inlet ratio, length–diameter aspect ratio, and wall roughness of the nozzle on the spatial distribution of pressure and velocity were studied.

2. CFD Model and Numerical Solution

Due to the sudden change of the flow area in the sudden expansion nozzles, the pressure in the nozzles changes dramatically, and the flow process of gas extinguishing agents in the expansion nozzles is a particularly complex gas–liquid two-phase flow. Williamson [31] found that the flow of Halon 1301 agent in the pipeline was accompanied by a large number of bubbles less than 0.01 inches in diameter, which is a typical dispersed bubbly flow. Therefore, the mixture model, which is suitable for computation bubbly flows where the gas volume fraction remains low [32], was selected for the simulation calculation of the release characteristics of the gas extinguishing agent in this study.

2.1. Governing Equations

To simplify the numerical calculation process, we made the following assumptions:

- (a) The carrier nitrogen in gas–liquid two-phase flow is regarded as ideal gas, and its dissolution in the liquid extinguishing agent is ignored.
- (b) The gaseous Halon 1301 extinguishing agent is also regarded as ideal gas.
- (c) The inner walls of the pipeline and the nozzle are adiabatic.

According to the above assumptions, the governing equations for the model are as follows:

Continuity equation:

$$\frac{\partial}{\partial t}(\rho_m) + \nabla \cdot (\rho_m \vec{v}_m) = 0 \quad (1)$$

Momentum equation:

$$\frac{\partial}{\partial t}(\rho_m \vec{v}_m) + \nabla \cdot (\rho_m \vec{v}_m \vec{v}_m) = -\nabla P + \nabla \cdot [\mu_m (\nabla \vec{v}_m + \nabla \vec{v}_m^T)] + \rho_m \vec{g} + \vec{F} + \nabla \cdot (\sum_{k=1}^n \alpha_k \rho_k \vec{v}_{dr,k} \vec{v}_{dr,k}) \quad (2)$$

Energy equation:

$$\frac{\partial}{\partial t} \sum_{k=1}^n (\alpha_k \rho_k E_k) + \nabla \cdot \sum_{k=1}^n (\alpha_k \vec{v}_k (\rho_k E_k + P)) = \nabla \cdot (k_{eff} \nabla T) + S_E \quad (3)$$

In the formulas, $\rho_m = \sum_{k=1}^n \alpha_k \rho_k$ is the mixture density; $\vec{v}_m = \frac{\sum_{k=1}^n \alpha_k \rho_k \vec{v}_k}{\rho_m}$ is the mass-averaged velocity; α_k is the volume fraction of phase k ; ρ_k is the density of phase k ; \vec{v}_k is the velocity of phase k ; n is the number of phases; \vec{F} is a body force; $\mu_m = \sum_{k=1}^n \alpha_k \mu_k$ is the viscosity of the mixture; $\vec{v}_{dr,k} = \vec{v}_k - \vec{v}_m$ is the drift velocity for secondary phase k ; $k_{eff} = \sum_{k=1}^n \alpha_k (k_k + k_t)$ is the effective thermal conductivity; k_t is the turbulent thermal conductivity, which is defined according to the turbulence model being used; $E_k = h_k - \frac{p}{\rho_k} + \frac{\vec{v}_k^2}{2}$ for a compressible phase, and $E_k = h_k$ for an incompressible phase, where h_k is the sensible enthalpy for phase k ; and S_E denotes the source term, which includes any other volumetric heat sources.

Since only one of the phases can be defined as a compressible ideal gas in the mixture model [32], in this study, the primary phase was set as the mixture of nitrogen and gaseous Halon 1301 extinguishing agent whose density was set as ideal-gas. The secondary phase was set as the liquid Halon 1301 extinguishing agent, which is incompressible; its density was set as piecewise-linear, and the relationship between density and temperature was expressed by 19 points in the present study. The volume fraction equation for the secondary phase l is as follows:

$$\frac{\partial}{\partial t} (\alpha_l \rho_l) + \nabla \cdot (\alpha_l \rho_l \vec{v}_l) = \dot{m}_{vl} - \dot{m}_{lv} \quad (4)$$

In the formula, \dot{m}_{vl} and \dot{m}_{lv} denote the interphase mass transfer rates from gas phase to liquid phase and from liquid phase to gas phase, respectively. The evaporation and condensation processes are as follows [33]:

The condensation process ($T < T_{sat}$) can be expressed as:

$$\dot{m}_{vl} = r_c \alpha_v \rho_v \frac{T - T_{sat}}{T_{sat}} \quad (5)$$

The evaporation process ($T > T_{sat}$) can be expressed as:

$$\dot{m}_{lv} = r_e \alpha_l \rho_l \frac{T - T_{sat}}{T_{sat}} \quad (6)$$

In the formulas, T_{sat} denotes the saturation temperature of the extinguishing agent; r_c and r_e represent the time relaxation factors to adjust the rate of phase transition, their values were both set as 100 [34]; α_v and α_l are the volume fractions of gas phase and liquid phase, respectively; and ρ_v and ρ_l represent the gas and liquid density, respectively.

2.2. Turbulence Model

The $k - \epsilon$ model has been widely used in ultrasonic turbulent flows, such as gas flows in Laval nozzles, and the reliability has been validated in many such kinds of simulations [20]. Moen et al. [35] studied the accuracy of the three well-known RANS eddy viscosity models, namely, standard $k - \epsilon$ model, re-normalization group (RNG) $k - \epsilon$ model, and realizable $k - \epsilon$ model, in typical gas release scenarios, including dense CO₂ release, impinging hydrogen jet, and a dense chlorine jet release. They found that the performance of the realizable $k - \epsilon$ model is substantially better than that of the other two $k - \epsilon$ models for the simulation of dense-phase gas releases. In particular, the realizable $k - \epsilon$ model predicts

the spreading rate for axisymmetric round-jets well, which is noteworthy. Therefore, in this study, the realizable $k - \varepsilon$ model was selected for the turbulence simulations. The modeled transport equations for k and ε are as follows [32]:

$$\frac{\partial}{\partial t}(\rho k) + \nabla \cdot \left(\rho k \vec{v} - \left(\mu + \frac{\mu_t}{\sigma_k} \right) \nabla \cdot k \right) = G_k + G_b - \rho \varepsilon - Y_M + S_k \quad (7)$$

and

$$\frac{\partial}{\partial t}(\rho \varepsilon) + \nabla \cdot \left(\rho \varepsilon \vec{v} - \left(\mu + \frac{\mu_t}{\sigma_\varepsilon} \right) \nabla \cdot \varepsilon \right) = \rho C_1 S \varepsilon - \rho C_2 \frac{\varepsilon^2}{k + \sqrt{\nu \varepsilon}} + C_{1\varepsilon} \frac{\varepsilon}{k} C_{3\varepsilon} G_b + S_\varepsilon \quad (8)$$

where

$$C_1 = \max \left[0.43, \frac{\eta}{\eta + 5} \right], \eta = S \frac{k}{\varepsilon}, S = \sqrt{2 S_{ij} S_{ij}}.$$

In the equations, G_k represents the generation of turbulence kinetic energy due to the mean velocity gradients; G_b denotes the generation of turbulence kinetic energy due to buoyancy; Y_M is the contribution of the fluctuating dilatation in compressible turbulence to the overall dissipation rate; $C_{1\varepsilon}$, C_2 and $C_{3\varepsilon}$ are constants; and σ_k and σ_ε are the turbulent Prandtl numbers for k and ε , respectively.

2.3. Computational Geometry and Grid

As shown in Figure 1a, the sudden-expansion nozzle was threaded on one end of a circular pipe with an inner diameter D_1 (inlet diameter) of 14.10 mm, and the length L_1 of the pipeline is 250 mm. Figure 1b shows the structure of the nozzle. The outlet–inlet area ratio ($\delta = A_2/A_1$) of the fire extinguishing nozzle varied from 1.25 to 5.00, with corresponding inner diameter D_2 (outlet diameter) of the nozzle varied from 15.76 mm to 31.53 mm. According to Li's [36] study, the optimal cavity length to the nozzle diameter is 3 for abrasive waterjet nozzles. Therefore, in this study, the range of L_2/D_2 aspect ratio was set as 0.50 to 3.00. In order to accurately obtain the exit condition of the fire extinguishing nozzle, we took the center point of the interface between the fire extinguishing nozzle and the pipeline (hereinafter referred to as “the changing interface”) as the coordinate origin, and the positive direction of the Z-axis went straight along the pipeline toward the pipeline inlet, as shown in Figure 1a. The space rectangular coordinate system was established.

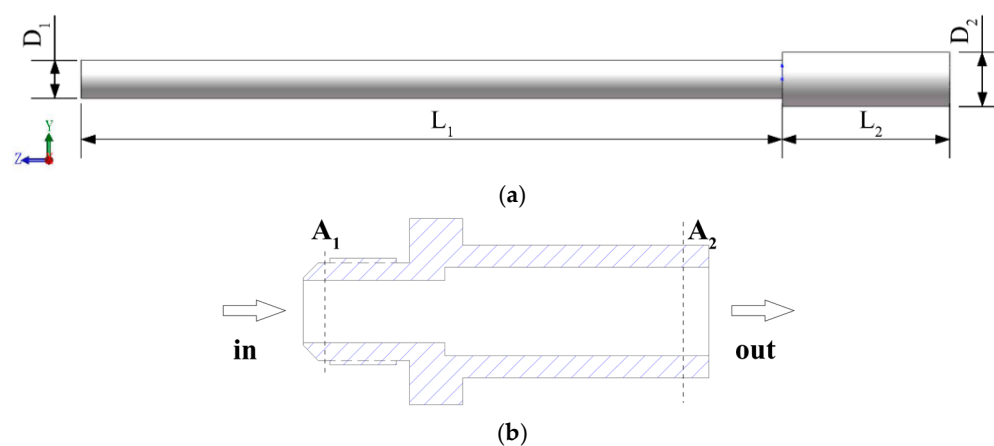


Figure 1. Structural diagram of the model: (a) nozzle and pipeline; (b) profile of nozzle.

The whole simulation model is shown in Figure 2. Considering that the pipeline flow and the spatial motion of the extinguishing agent were approximately axisymmetric, the whole computational domain was designed as a cylinder with a radius of 350 mm and a length of 1240 mm. There was a circular wall added at the entrance side of the pipeline. The cylinder surface and the end face of the outlet side of the cylinder were set as the pressure outlet boundary, and the cylinder was filled with atmospheric nitrogen in order to

simulate the environmental conditions in which the fire extinguishing agent is sprayed to the atmospheric pressure.

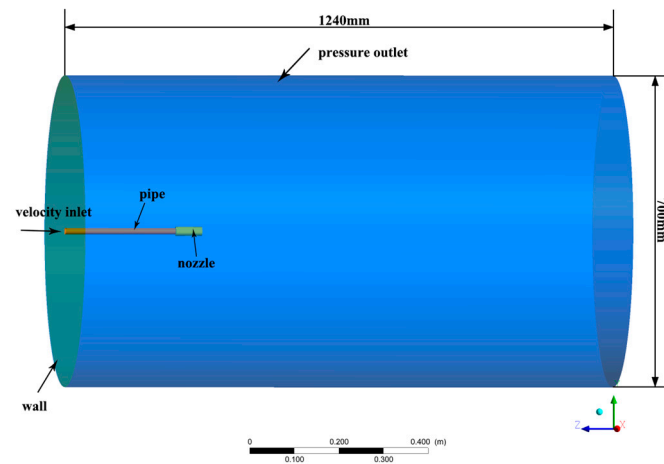


Figure 2. Structural diagram of the whole simulation model.

As shown in Figure 3a,b, the structured hexahedral mesh with high quality was adopted for domain discretization, and the grids within and near the nozzle and the pipeline were locally refined. In order to test the independence of the grids, the variation of the average pressure difference between the nozzle inlet and outlet sections with the number of grids was studied. The results are shown in Figure 4. As can be seen from Figure 4, when the number of grids reached 972,640, the average pressure difference did not change significantly with the increase of the number of grids. The difference between the pressure difference when the number of grids was 2,426,240 and that when the number of grids was 972,640 is about 3.6%. However, using a computer with Intel Xeon E5-2670 CPU, we found that the solution time of a single case increased dramatically from about 20 h to about 55 h. Therefore, considering the calculation cost and the grid sensitivity, we divided the calculation domain into 972,640 cells.

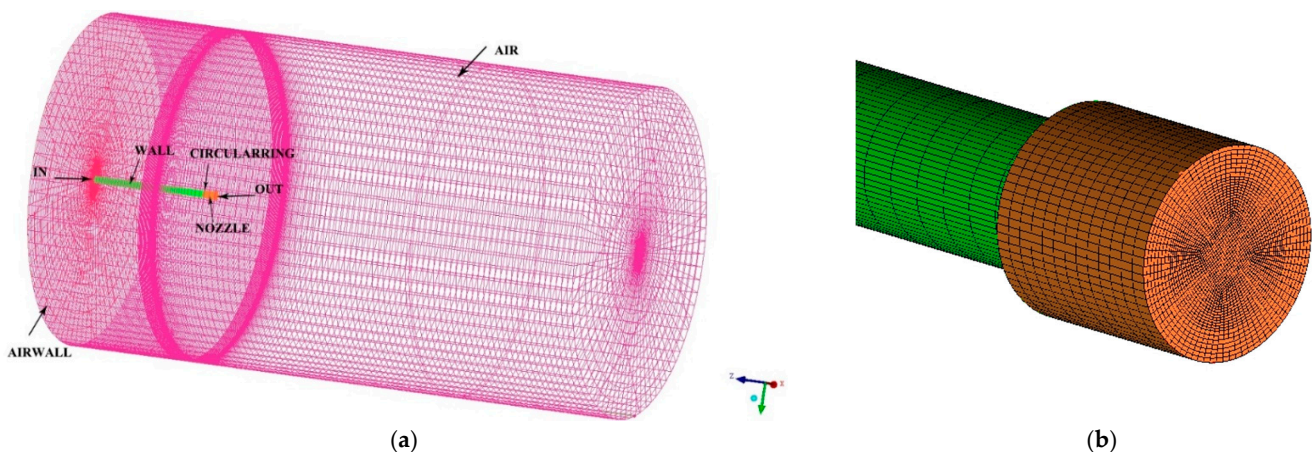


Figure 3. Diagram of grids: (a) overall view; (b) grids of nozzle.

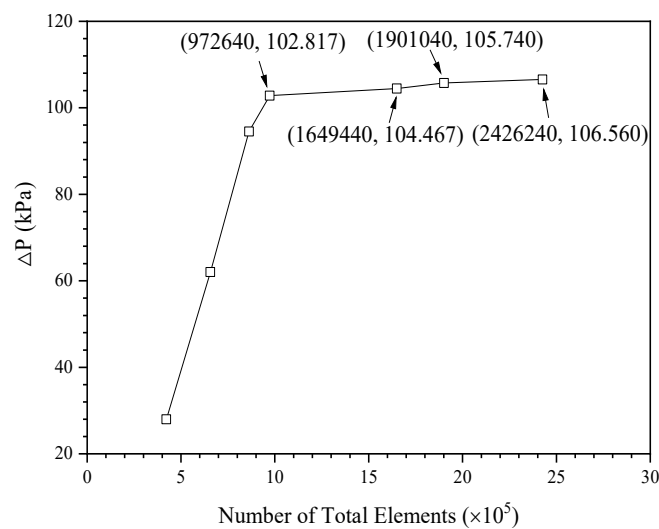


Figure 4. Mesh dependence study.

2.4. Boundary Conditions and Numerical Approach

In order to focus on the influence of the nozzle geometric parameters on the release characteristics of the extinguishing agent, we set the inlet boundary of the pipeline to a constant velocity inlet of 25 m/s in this study. The volume fractions of each component at the pipeline inlet were as follows: the liquid Halon 1301 accounted for 80%, the gaseous Halon 1301 accounted for 10%, and the remainder was nitrogen. The nozzle and pipeline walls were set as no-slip walls, whose materials were aluminum with wall roughness of 0.16 mm. The near wall region adopted a standard wall function approach. The initial temperature was 294.25 K. As an improved extension of the semi-implicit method for pressure-linked equations (SIMPLE), SIMPLEC is able to improve convergence for complicated flows when it is limited by the pressure–velocity coupling [37,38], and therefore it was employed for the treatment of the pressure–velocity coupling in the present study. Considering the fact that the PRESTO! (PREssure STaggering Option) scheme has good adaptability to high swirling flows and pressure rapid change flows [32,39], we adopted it for the discretization of the pressure term in this study. The terms of density, momentum, turbulent kinetic energy, and turbulent dissipation rate all discretized with the second order upwind scheme. For the transient formulation, the second-order implicit method was adopted for iteration convergence of the residuals.

2.5. Design of Simulate Conditions

In order to study the influence of the nozzle outlet–inlet area ratio (δ) on the flow and release characteristics of the sudden expansion nozzles, we carried out 12 groups of comparative tests under the same conditions of the inner diameter of the nozzle inlet (D_1), the ratio of the expansion section length to the inner diameter of the nozzle outlet ($\xi = L_2/D_2$), and the roughness of the pipeline and nozzle walls (ε_P and ε_N , respectively). The values of each parameter are shown in Table 1.

In order to reveal the influence of the ratio of the expansion section length to the inner diameter of the nozzle outlet ($\xi = L_2/D_2$) on the flow and release characteristics of the sudden expansion nozzles, we carried out six groups of comparative tests under the same conditions of the inner diameter of the nozzle inlet (D_1), the nozzle outlet–inlet area ratio (δ), and the roughness of the pipeline and nozzle walls (ε_P and ε_N , respectively). The values of each parameter are shown in Table 2.

Table 1. Geometric parameters of the simulation model under different area ratios.

Case No.	Area Ratio δ	Length–Diameter Ratio ζ	Pipeline Length L_1/mm	Inlet Diameter D_1/mm	Expansion Length L_2/mm	Outlet Diameter D_2/mm	Wall Roughness	
							ε_P/mm	ε_N/mm
1	1.25	3.00	250	14.10	47.29	15.76	0.16	0.16
2	1.30	3.00	250	14.10	48.23	16.08	0.16	0.16
3	1.40	3.00	250	14.10	50.05	16.68	0.16	0.16
4	1.50	3.00	250	14.10	51.81	17.27	0.16	0.16
5	1.75	3.00	250	14.10	55.96	18.65	0.16	0.16
6	2.00	3.00	250	14.10	59.82	19.94	0.16	0.16
7	2.50	3.00	250	14.10	66.88	22.29	0.16	0.16
8	3.00	3.00	250	14.10	73.27	24.42	0.16	0.16
9	3.50	3.00	250	14.10	79.14	26.38	0.16	0.16
10	4.00	3.00	250	14.10	84.60	28.20	0.16	0.16
11	4.50	3.00	250	14.10	89.73	29.91	0.16	0.16
12	5.00	3.00	250	14.10	94.59	31.53	0.16	0.16

Table 2. Geometric parameters of the simulation model under different length–diameter ratios.

Case No.	Area Ratio δ	Length–Diameter Ratio ζ	Pipeline Length L_1/mm	Inlet Diameter D_1/mm	Expansion Length L_2/mm	Outlet Diameter D_2/mm	Wall Roughness	
							ε_P/mm	ε_N/mm
13	3.00	0.50	250	14.10	12.21	24.42	0.16	0.16
14	3.00	1.00	250	14.10	24.42	24.42	0.16	0.16
15	3.00	2.00	250	14.10	48.84	24.42	0.16	0.16
16	3.00	2.50	250	14.10	61.05	24.42	0.16	0.16
8	3.00	3.00	250	14.10	73.27	24.42	0.16	0.16
17	3.00	4.00	250	14.10	97.69	24.42	0.16	0.16

In order to study the influence of the nozzle inner wall roughness (ε_N) on the flow and release characteristics of the sudden expansion nozzles, we carried out four groups of comparative tests under the same conditions of the inner diameter of the nozzle inlet (D_1), the nozzle outlet–inlet area ratio (δ), the ratio of the expansion section length to the inner diameter of the nozzle outlet ($\zeta = L_2/D_2$), and the roughness of the pipeline inner wall (ε_P). Considering that the roughness value of the industrial metal pipelines under non-corrosive conditions is usually less than 0.2 mm [40,41], in this study, the roughness of the inner wall of the nozzle was set as 0.14 mm, 0.16 mm, 0.18 mm, and 0.20 mm, respectively. The values of each parameter are shown in Table 3.

Table 3. Geometric parameters of the simulation model under different nozzle wall roughness.

Case No.	Area Ratio δ	Length–Diameter Ratio ζ	Pipeline Length L_1/mm	Inlet Diameter D_1/mm	Expansion Length L_2/mm	Outlet Diameter D_2/mm	Wall Roughness	
							ε_P/mm	ε_N/mm
18	3.00	3.00	250	14.10	73.27	24.42	0.16	0.14
8	3.00	3.00	250	14.10	73.27	24.42	0.16	0.16
19	3.00	3.00	250	14.10	73.27	24.42	0.16	0.18
20	3.00	3.00	250	14.10	73.27	24.42	0.16	0.20

3. Results and Discussion

The release of the gas extinguishing agent through nozzles is a typical considerably complex gas–liquid two-phase turbulent flow. That is, the gas extinguishing agent is not only constrained by the nozzle wall but also has significant heat exchange with the wall and obvious gasification phase transition. Therefore, the distribution characteristics of the extinguishing agent during the flow and release, such as the spatial distribution of pressure and velocity in the nozzle, are usually not completely symmetrical. Moreover,

their characteristics are inevitably affected by the geometric parameters of the nozzle such as outlet–inlet area ratio, length–diameter aspect ratio, and wall roughness, which will be discussed in the following sections.

3.1. Effects of Outlet–Inlet Area Ratio on the Release Characteristics

3.1.1. Effects of Outlet–Inlet Area Ratio on the Pressure Characteristics

The pressure distribution characteristics usually have a particularly important influence on the flow of the medium. Especially for the gas–liquid two-phase flow, the pressure distribution in the cavity will also significantly affect the gasification characteristics of the medium. Therefore, it is necessary to study the pressure distribution characteristics in the nozzle.

The section pressure distribution and 3D streamline images of the pipeline and nozzle under different outlet–inlet area ratios are shown in Figure 5. It can be seen from Figure 5 that there was an obvious pressure attenuation in the nozzle expansion section, and the overall apparent pressure in the expansion section decreased with the increase of the outlet–inlet area ratio δ . In addition, when $\delta \leq 1.5$, the pressure distribution in the nozzle presented a cone-shaped structure with the vertex heading towards the nozzle outlet, and the overall pressure in the cone-shaped region decreased with the increase of δ . In addition, the pressure in the other regions of the nozzle was significantly smaller than that in the conical area. The shape of the corresponding streamlines in the pipeline and nozzle was approximately linear, and no obvious turning phenomenon occurred in the area mutation region. This may have been due to the fact that when $\delta \leq 1.5$, the cross-sectional area of the nozzle was not much different from that of the pipeline, and the expansion of the medium in the expansion section of the nozzle was not very obvious; thus, there was no great change in the structure of the fluid.

When $\delta > 1.5$, the conical structure moved from the nozzle interior along the opposite direction of the flow to the region near the nozzle in the pipeline, and a cone-shaped low-pressure region began to appear near the area mutation region, with the area of the low-pressure region increasing with the increase of δ . Moreover, when $\delta = 5$, another small low-pressure region appeared downstream of the cone-shaped low-pressure region inside the nozzle. The corresponding streamlines in the nozzle showed a turning phenomenon, obvious expansion occurred in the sudden expansion area, and the expansion amplitude increased with the increase of δ . This may have been due to the fact that the fluid usually expands when it flows through the expanding area [42]. This expansion may reduce the local pressure and accelerate the gasification rate of the gas extinguishing agent, which may induce vortices and increase the local resistance loss, and then superimposes the compression effect of the pressure waves reflected by the inner walls of the nozzle so the flow in the nozzle presented a structure similar to the under-expanded jet.

In order to facilitate the analysis of the pressure distribution characteristics during the flow process, as shown in Figure 6a, we plotted the variation curves of the pressure on the central axis of the pipeline and the nozzle under different outlet–inlet area ratios. It can be seen from Figure 6a that the pressure distribution curves on the central axis under different area ratios were significantly different. Specifically, when $\delta \leq 1.5$, as shown by the black dotted ellipse in the figure, the sudden drop of the pressure on the central axis (corresponding to the conical region in the cloud image) occurred on the side of the nozzle, and the pressure decreased monotonically along the axial direction in the nozzle. However, when $\delta > 1.5$, as shown by the blue dotted ellipse in Figure 6a, the sudden pressure drop appeared on the side of the pipeline. Moreover, the pressure on the central axis showed an obvious non-monotonic change, which decreased first and then increased in the region close to the sudden increase of area, as shown by the red dotted ellipse in the figure. In fact, the minimum pressure here happened to occur at the core of the aforementioned cone-shaped low-pressure zone.

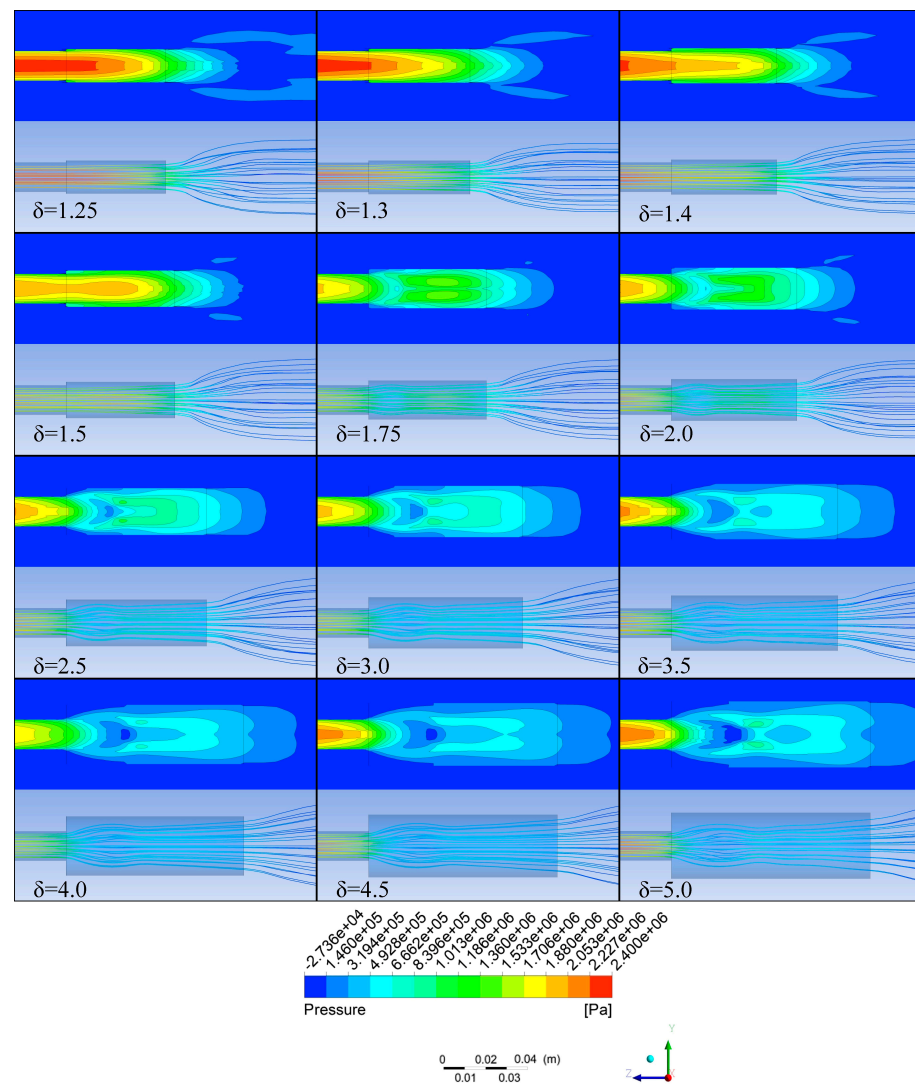


Figure 5. Section pressure distribution and 3D streamlines under different area ratios.

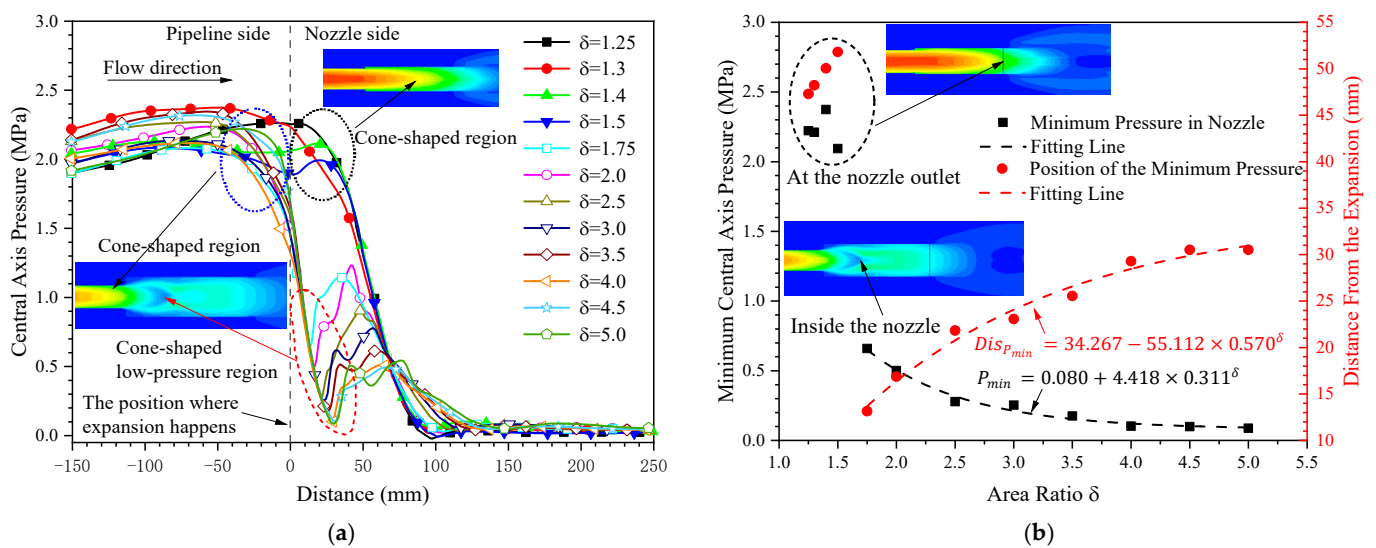


Figure 6. Cont.

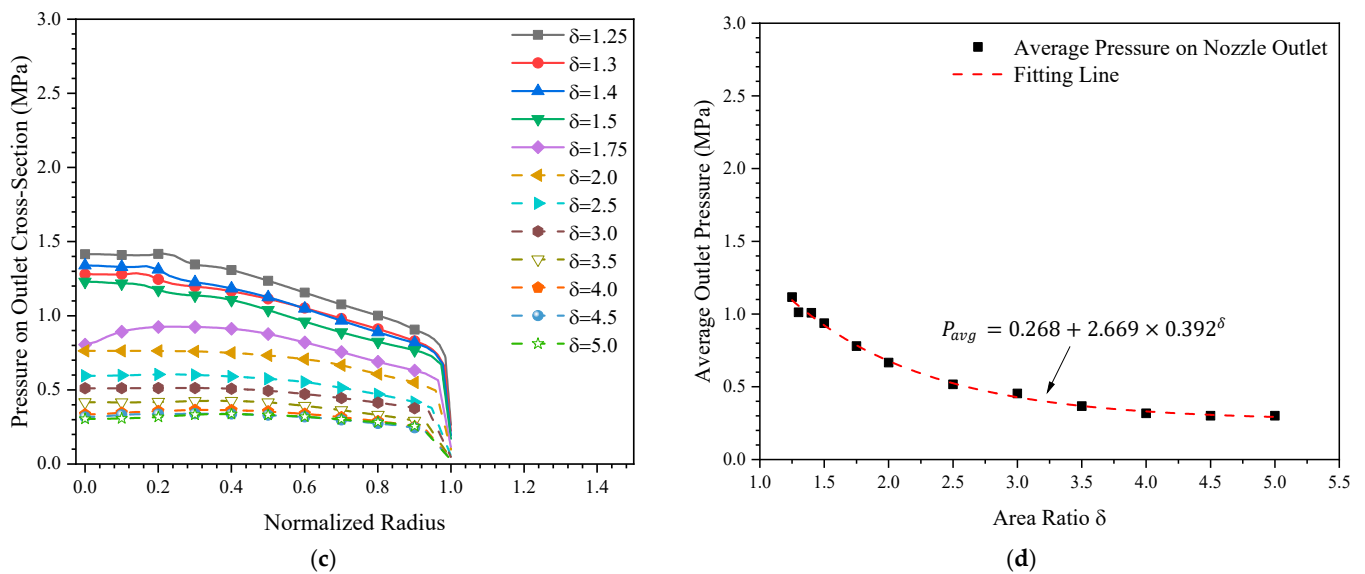


Figure 6. Variation of pressure under different area ratios: (a) central axis pressure curves; (b) minimum pressure and distance; (c) pressure variation with the radius; (d) average pressure on the nozzle outlet cross-section.

Figure 6b shows the variations of the minimum pressure on the central axis in the nozzle (P_{min}) and the distance of the position where the minimum pressure appeared from the position where the area expansion occurred ($Dis_{P_{min}}$) vs. δ . It can be seen from Figure 6b that the variation of P_{min} and $Dis_{P_{min}}$ with δ can be clearly divided into two parts, namely, when $\delta \leq 1.5$, the value of P_{min} was relatively large, and since the corresponding position of P_{min} only appeared at the outlet cross-section of the nozzle, the value of $Dis_{P_{min}}$ was also relatively large; when $\delta > 1.5$, with the increase of δ , the value of P_{min} decreased monotonically, while the value of $Dis_{P_{min}}$ increased gradually. They can be fitted by exponential functions, and the fitting results are shown in Equations (9) and (10).

$$P_{min} = 0.080 + 4.418 \times 0.311^\delta \quad (9)$$

$$Dis_{P_{min}} = 34.267 - 55.112 \times 0.570^\delta \quad (10)$$

where P_{min} represents the minimum pressure in the nozzle (Mpa); $Dis_{P_{min}}$ denotes the distance of the position where the minimum pressure appears from the position where the area expansion happens (mm); and δ represents the outlet-inlet area ratio of the nozzle.

From the above analysis, it can be seen that the increase of δ will significantly affect the pressure distribution in the nozzle, especially in the region of sudden expansion, and there was a local low-pressure zone in the nozzle, which may lead to the acceleration of the gasification rate of the gas extinguishing agent and may likely induce strong vortices inside the flow field, eventually making the flow field structure change significantly.

In order to analyze the influence of δ on the pressure on the nozzle outlet, as shown in Figure 6c, we plotted the variation of the pressure on the outlet cross-section of the nozzle with the normalized radius (distance from the central axis divided by the radius of the outlet cross-section) against δ . It can be seen from Figure 6c that the overall pressure on the outlet cross-section decreased with the increase of the area ratio, and the uniformity of the pressure distribution along the radial direction was obviously improved when $\delta \geq 2$. This may have been due to the fact that the relatively large outlet-inlet area ratio under the same length-diameter aspect ratio made the extinguishing agent expand violently in the nozzle cavity and made it fully turbulent.

Figure 6d shows the average pressure on the nozzle outlet cross-section (P_{avg}) vs. δ . It can be seen from Figure 6d that P_{avg} decreased monotonically with the increase of δ . This may have been due to the fact that, on the one hand, when the discharge driving force is constant, the increase in the export cross-section area will inevitably reduce the overall

pressure; on the other hand, the continuous increase in the flow area makes the flow field structure in the nozzle undergo a fundamental change, which makes the uniformity of the pressure distribution of the nozzle outlet cross-section significantly improved. The change of P_{avg} can be fitted by an exponential function, and the results are shown in Equation (11).

$$P_{avg} = 0.268 + 2.669 \times 0.392^\delta \quad (11)$$

where P_{avg} represents the average pressure on the cross-section of the nozzle outlet (Mpa), and δ denotes the outlet–inlet area ratio of the nozzle.

3.1.2. Effects of Outlet–Inlet Area Ratio on the Velocity Characteristics

The flow velocity is an important parameter to characterize the release characteristics of nozzles, not only affecting the release rate of the nozzle but also affecting the spatial motion and diffusion characteristics of the medium after spraying out of the nozzle. Therefore, it is necessary to further study the velocity distribution characteristics in the nozzle.

Figure 7 shows the section velocity distribution and 3D streamline images of the pipeline and nozzle under different outlet–inlet area ratios. It can be seen from Figure 7 that the velocity inside the nozzle varied with the increase of the area ratio. When $\delta \leq 1.5$, the velocity change in the nozzle was not significant, and the streamlines were approximately straight. However, when $\delta = 1.75$, a local high-speed zone with significantly increased velocity appeared, and the bending deformation of the streamlines appeared near the area mutation region in the nozzle, with both the area of this region and the amplitude of the bending deformation increasing with the increase of the area ratio. In addition, there was an obvious local low-speed region in the downstream of the high-speed zone, and its area also increased with the increase of the area ratio. This may have been due to the fact that when the area ratio was relatively large, the extinguishing agent had a significant expansion when it flowed through the area mutation region, which formed significant local vortices in the wall attachment of the area mutation region. The flow field inside the nozzle presented the characteristics of a typical under-expanded jet, and its intensity increased with the increase of δ . Moreover, due to the continuous energy consumption during the flow, the intensity of the downstream under-expanded jet was significantly weakened.

In order to facilitate the analysis of the velocity distribution characteristics during the flow process, as shown in Figure 8a, we plotted the variation curves of the velocity on the central axis towards the nozzle outlet direction under different outlet–inlet area ratios. It can be seen from Figure 8a that in the region near the area mutation of the nozzle, the velocity on the central axis presented two kinds of obviously different trends with δ , as shown in the solid lines and imaginary lines, respectively. Specially, when $\delta \leq 1.5$, the velocity on the central axis changed little in the area mutation region. However, when $\delta > 1.5$, there was a significant peak of the velocity on the central axis near the area mutation region in the nozzle, and the value and width of the peak increased with the increase of δ . Moreover, an obvious valley appeared in the downstream region of the peak. This shows that the axial velocity in the area mutation region had obvious oscillations, which should be related to the transformation of the flow field structure into under-expanded flow.

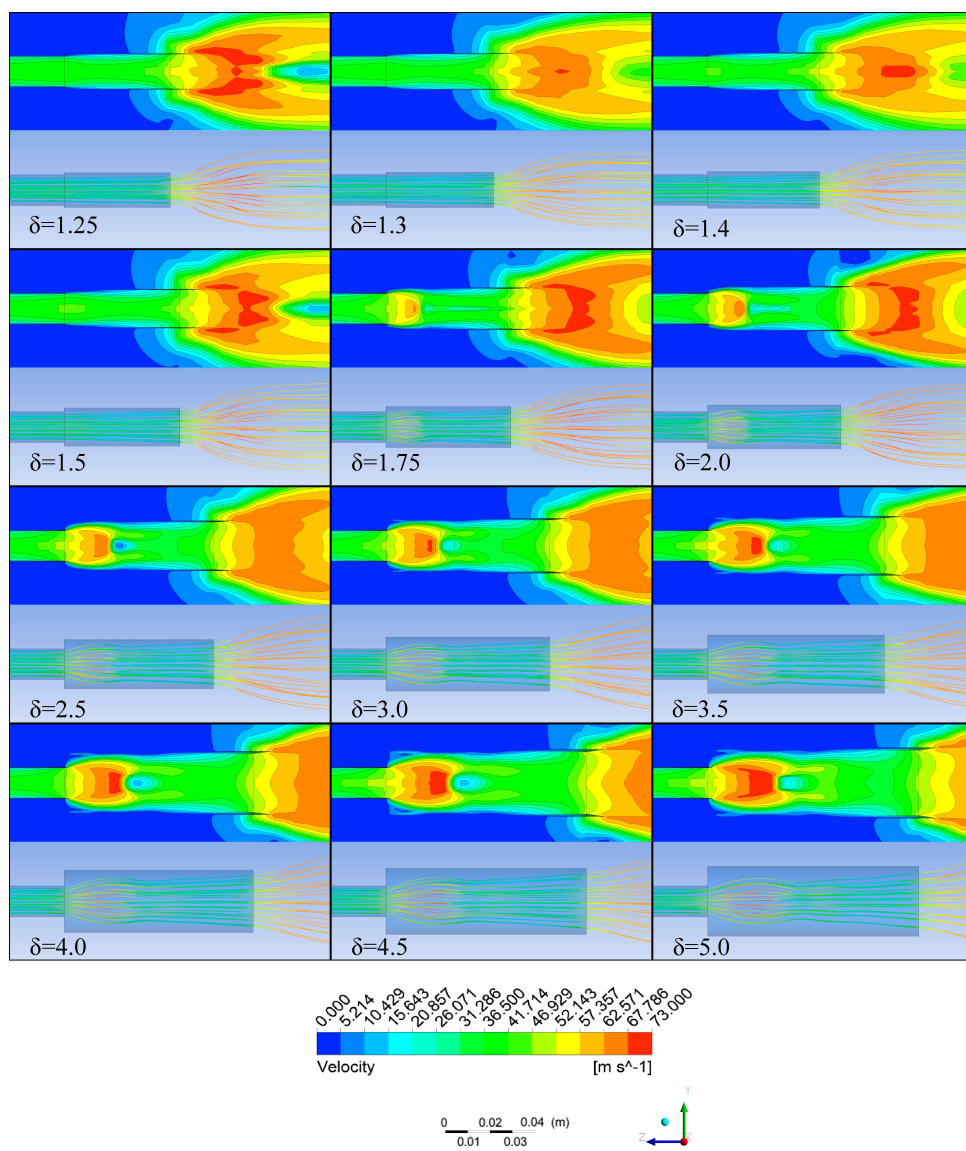


Figure 7. Section velocity distribution and 3D streamlines under different area ratios.

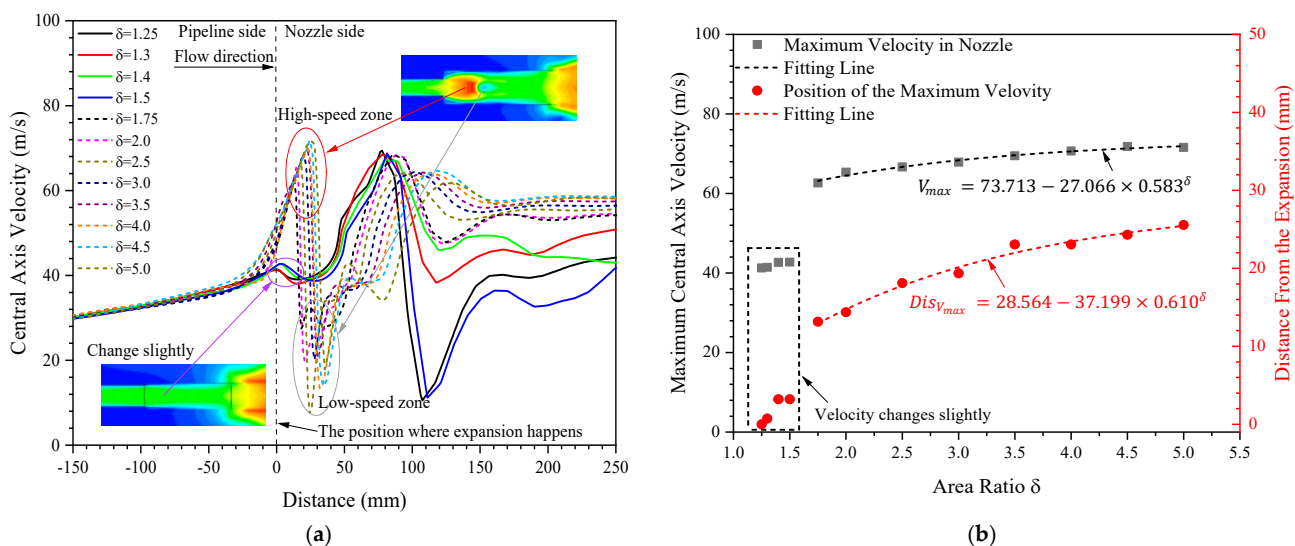


Figure 8. Cont.

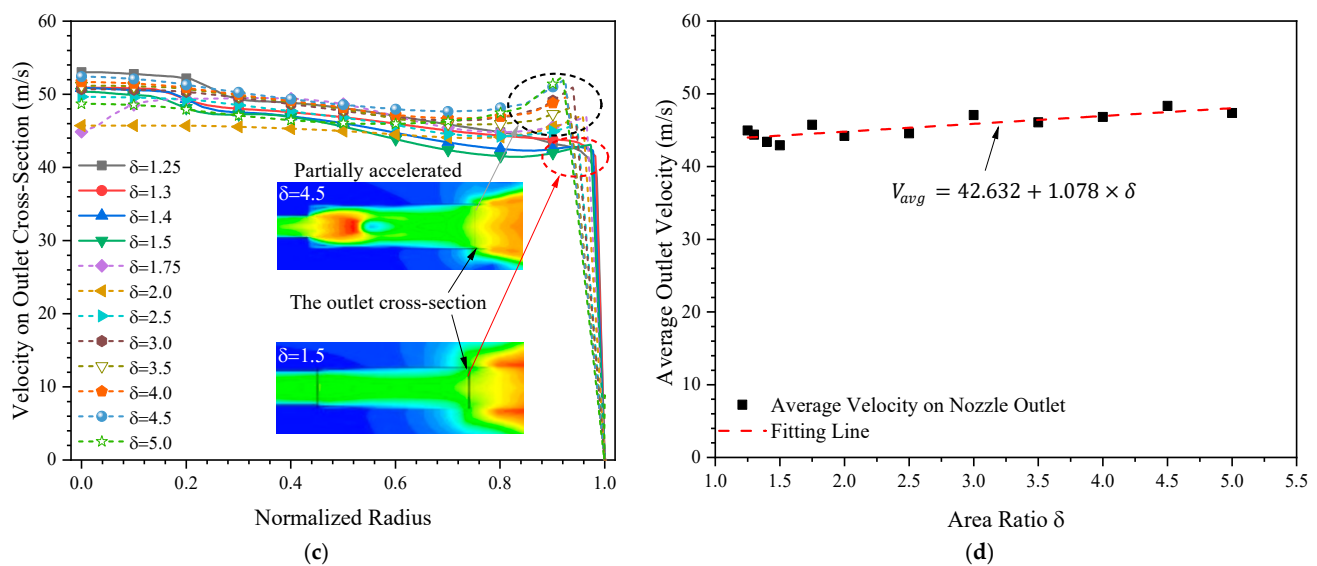


Figure 8. Variation of axial velocity under different area ratios: (a) central axis velocity curves; (b) maximum velocity and distance; (c) velocity variation with the radius; (d) average velocity on the nozzle outlet cross-section.

Figure 8b shows the variations of the maximum velocity on the central axis in the nozzle (V_{max}) and the distance of the position where the maximum pressure appeared from the position where the area expansion occurred ($Dis_{V_{max}}$) vs. δ . It can be seen from Figure 8b that the variation of V_{max} and $Dis_{V_{max}}$ with δ can also be clearly divided into two parts, namely, when $\delta \leq 1.5$, the value of V_{max} was relatively small, and the value of $Dis_{V_{max}}$ was also relatively small; when $\delta > 1.5$, the values of V_{max} and $Dis_{V_{max}}$ both increased with the increase of δ . They can be fitted by exponential functions, and the fitting results are shown in Equations (12) and (13).

$$V_{max} = 73.713 - 27.066 \times 0.583^{\delta} \quad (12)$$

$$Dis_{V_{max}} = 28.564 - 37.199 \times 0.610^{\delta} \quad (13)$$

where V_{max} represents the maximum velocity in the nozzle (m/s); $Dis_{V_{max}}$ denotes the distance of the position where the maximum velocity appears from the position where the area expansion happens (mm); and δ represents the outlet–inlet area ratio of the nozzle.

In order to analyze the influence of δ on the axial velocity at the nozzle outlet, as shown in Figure 8c, we plotted the variation of the axial velocity on the outlet cross-section of the nozzle with the normalized radius against δ . As shown in Figure 8c, the overall variation of the axial velocity on the outlet cross-section with δ was small, and the uniformity of the axial velocity distribution along the radial direction increased slightly with the increase of δ . In addition, when $\delta > 1.5$, the axial velocity on the outlet cross-section near the inner surface of the nozzle was significantly larger than that when $\delta \leq 1.5$. This may have been related to the increase of turbulence intensity in the near-wall region.

Figure 8d shows the average axial velocity on the nozzle outlet cross-section (V_{avg}) vs. δ . As shown in Figure 8d, within the value range of δ in this study, the changes of V_{avg} were relatively small, and generally V_{avg} was of a slow increase trend with the increase of δ . It can be fitted by a linear function, and the results are shown in Equation (14).

$$V_{avg} = 42.632 + 1.078 \times \delta \quad (14)$$

where V_{avg} represents the average axial velocity on the cross-section of the nozzle outlet (m/s), and δ denotes the outlet–inlet area ratio of the nozzle.

3.2. Effects of Length–Diameter Aspect Ratio on the Release Characteristics

3.2.1. Effects of Length–Diameter Aspect Ratio on the Pressure Characteristics

Figure 9 shows the section pressure distribution and 3D streamline images of the pipeline and nozzle under different length–diameter aspect ratios. It can be seen from Figure 9 that compared with the inlet pressure of the nozzle, the overall pressure in the sudden expansion zone was significantly reduced. When $\xi > 1$, an obvious conical low-pressure zone, for which area increased first and then decreased with the increase of ξ , appeared in the nozzle near the expansion area. In addition, the streamlines in the corresponding region shrunk after expansion. This may have been due to the reflection of the pressure by the inner wall of the nozzle. In addition, when $\xi > 2$, multiple low-pressure zones with different intensities appeared in the nozzle along the flow direction, and these low-pressure zones became more and more obvious with the increase of ξ . This may have been due to the fact that the length of the expansion section increased with the increase of ξ , which made the vaporized extinguishing agents have the constraint condition of significantly compressing the subsequent fluid in the expansion section. In addition, the increase of the length of the expansion section created favorable conditions for the pressure reflection of the nozzle wall, and therefore the flow in the nozzle presented a typical under-expanded flow structure.

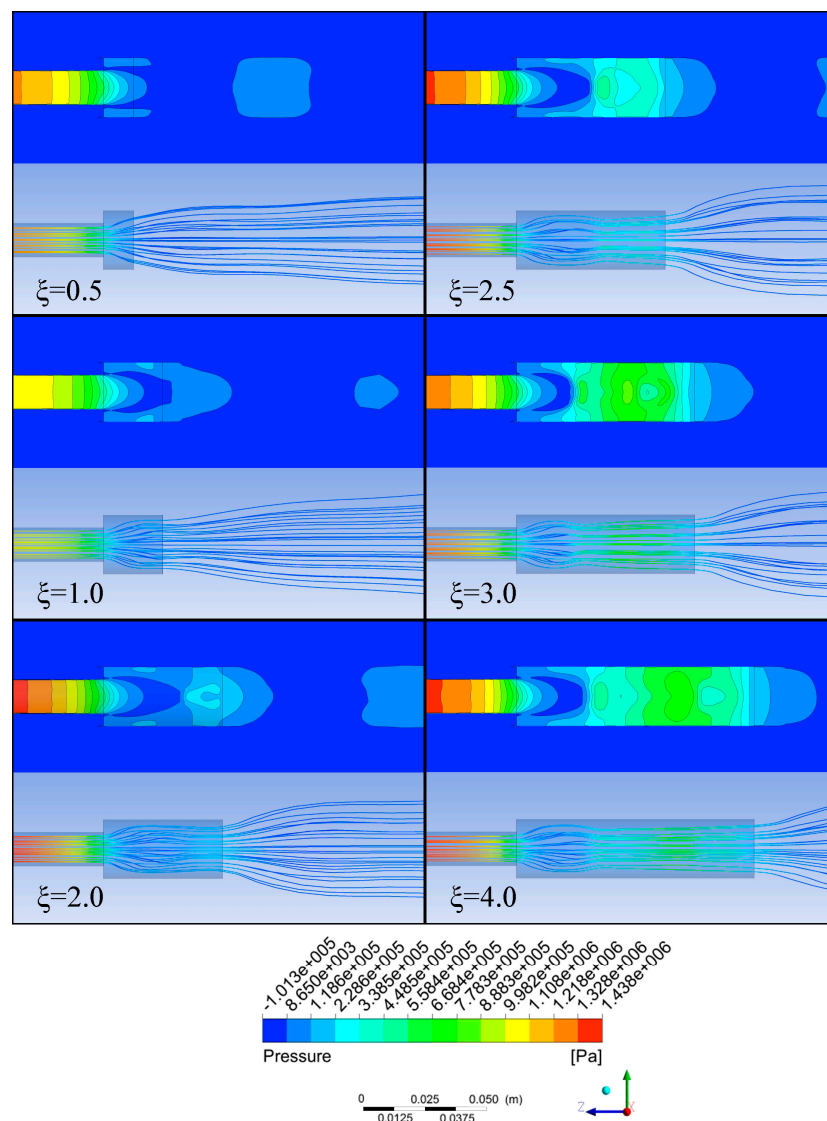


Figure 9. Section pressure distribution and 3D streamlines under different length–diameter ratios.

Figure 10a shows the variation curves of the pressure on the central axis of the pipeline and the nozzle under different length–diameter aspect ratios. It can be seen from Figure 10a that the pressure distribution curves on the central axis under different length–diameter aspect ratios (ζ) were significantly different. Specifically, as shown by the black dotted ellipse in the figure, when $\zeta < 2$, the minimum pressure on the central axis appeared outside of the nozzle. On the other hand, when $\zeta \geq 2$, the minimum pressure on the central axis appeared inside of the nozzle, and, remarkably, repeated pressure rise and fall appeared on the axial pressure curves (as shown by dotted lines in the figure) inside of the nozzle. This also showed that the fluid in the expansion section of the nozzle presented an under-expanded flow structure.

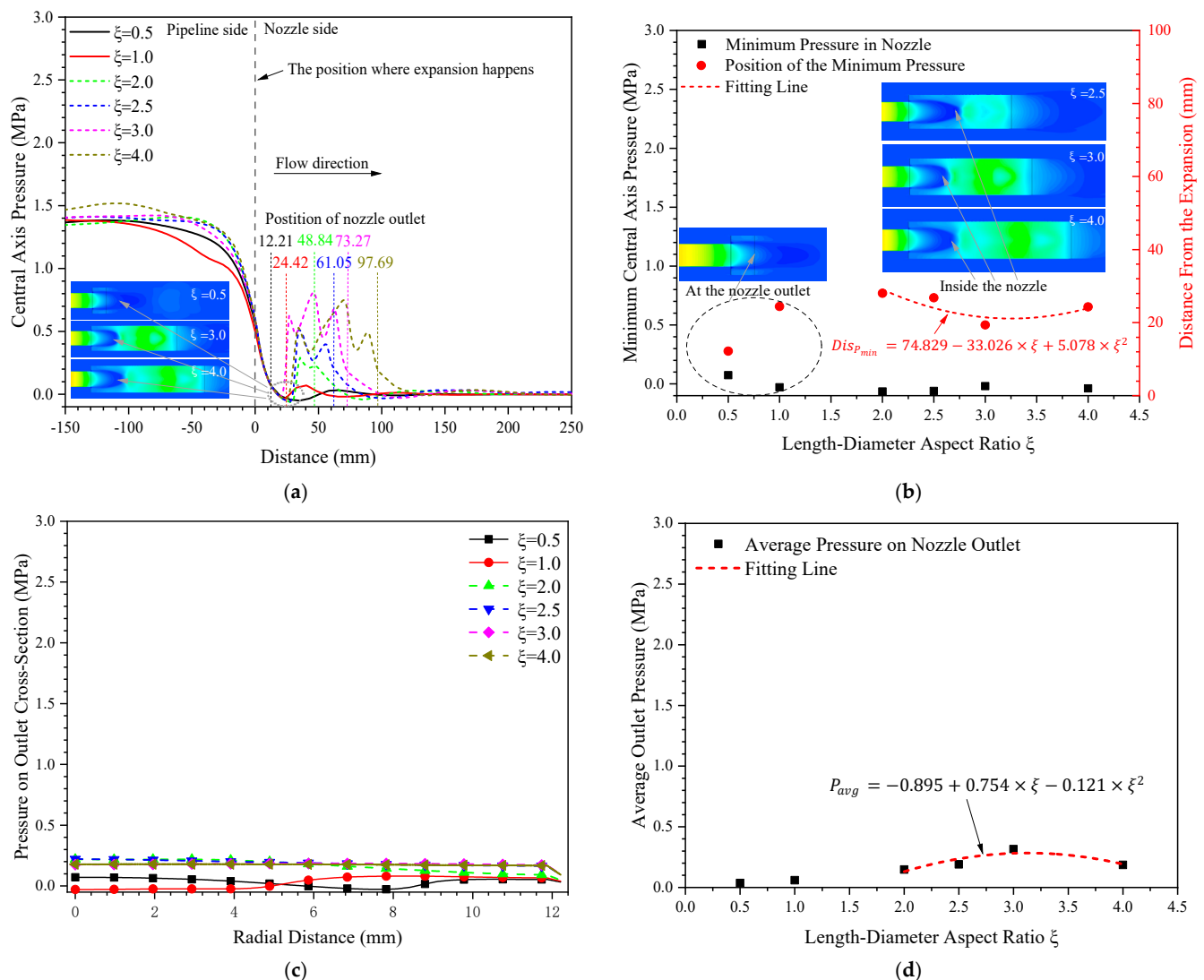


Figure 10. Variation of pressure under different length–diameter aspect ratios: (a) central axis pressure curves; (b) minimum pressure and distance; (c) pressure variation with the radius; (d) average pressure on the nozzle outlet cross-section.

Figure 10b shows the variations of the minimum pressure on the central axis in the nozzle (P_{min}) and the distance of the position where the minimum pressure appeared from the position where the area expansion occurred ($Dis_{P_{min}}$) vs. ζ . It can be seen from Figure 10b that the variation of P_{min} and $Dis_{P_{min}}$ with ζ could be clearly divided into two parts, namely, when $\zeta < 2$, since the corresponding position of P_{min} only appeared at the outlet cross-section of the nozzle, the value of P_{min} was relatively large; when $\zeta \geq 2$, with the increase of ζ , the value of P_{min} was close to zero and its change range was small,

while the value of $Dis_{P_{min}}$ decreased first and then increased. It can be fitted by a quadratic polynomial function, as shown in Equation (15).

$$Dis_{P_{min}} = 74.829 - 33.026 \times \zeta + 5.078 \times \zeta^2 \quad (15)$$

where $Dis_{P_{min}}$ denotes the distance of the position where the minimum pressure appeared from the position where the area expansion occurred (mm); ζ represents the length–diameter aspect ratio of the nozzle.

From the above analysis, it can be seen that the increase of ζ also significantly affected the pressure distribution in the nozzle. This may have been due to the fact that the extension of the expansion section made the flow of the extinguishing agent constrained, which could facilitate the formation of the vortex and increase its strength in the expansion section so that the structure of the flow in the nozzle changes significantly.

In order to analyze the influence of ζ on the pressure at the nozzle outlet, as shown in Figure 10c, we plotted the variation of the pressure on the outlet cross-section of the nozzle with the radius against ζ . It can be seen from the figure that the overall pressure on the outlet cross-section was relatively small, and when $\zeta > 2$, the pressure on the outlet cross-section was close to uniform distribution, which indicated that the flow in the expansion section was fully turbulent and the gaseous and liquid extinguishing agents were fully mixed.

Figure 10d shows the average pressure on the nozzle outlet cross-section (P_{avg}) vs. ζ . It can be seen from the figure that P_{avg} was close to zero (gauge pressure) when $\zeta < 2$; this may have been due to the fact that the expansion section was too short, and therefore the fire extinguishing agent was sprayed into the atmosphere before it was fully vaporized. However, when $\zeta \geq 2$, with the increase of ζ , P_{avg} increased slightly first and then decreased slightly. The slight increase of P_{avg} in front may have been related to the increase of gasification amount of the extinguishing agent in the expansion section, while the slight decrease in the back may have been caused by the increase of the flow resistance. Moreover, the change of P_{avg} when $\zeta \geq 2$ can be fitted by a quadratic polynomial function, and the fitting result is shown in Equation (16).

$$P_{avg} = -0.895 + 0.754 \times \zeta - 0.121 \times \zeta^2 \quad (16)$$

where P_{avg} represents the average pressure on the cross-section of the nozzle outlet (Mpa), and ζ denotes the length–diameter aspect ratio of the nozzle.

3.2.2. Effects of Length–Diameter Aspect Ratio on the Velocity Characteristics

Figure 11 shows the section velocity distribution cloud images and the 3D streamlines under different length–diameter aspect ratios. It can be seen from the cloud images that there was a conical high-velocity region near the expansion area, and the size of the conical region and its relative position with the nozzle outlet were significantly different with the increase of the length–diameter aspect ratio ζ .

Specifically, when $\zeta < 2$, the conical region extended beyond the nozzle outlet; however, when $\zeta \geq 2$, the whole conical region appeared within the expansion section of the nozzle, and the area of the conical region decreased first and then increased slightly with the increase of ζ . This may have been due to the fact that when ζ is relatively small, the length of the expansion section is too short, and therefore the extinguishing agent rushes out of the expansion section before it is fully diffused. However, when ζ is relatively large, the length of the expansion section can meet the needs of the development of the diffusion of the extinguishing agent. Alongside Figure 10d, it can be seen that as ζ increased, the average pressure on the nozzle outlet cross-section increased first and then decreased, which should be the reason that the size of the aforementioned conical area decreased first and then increased.

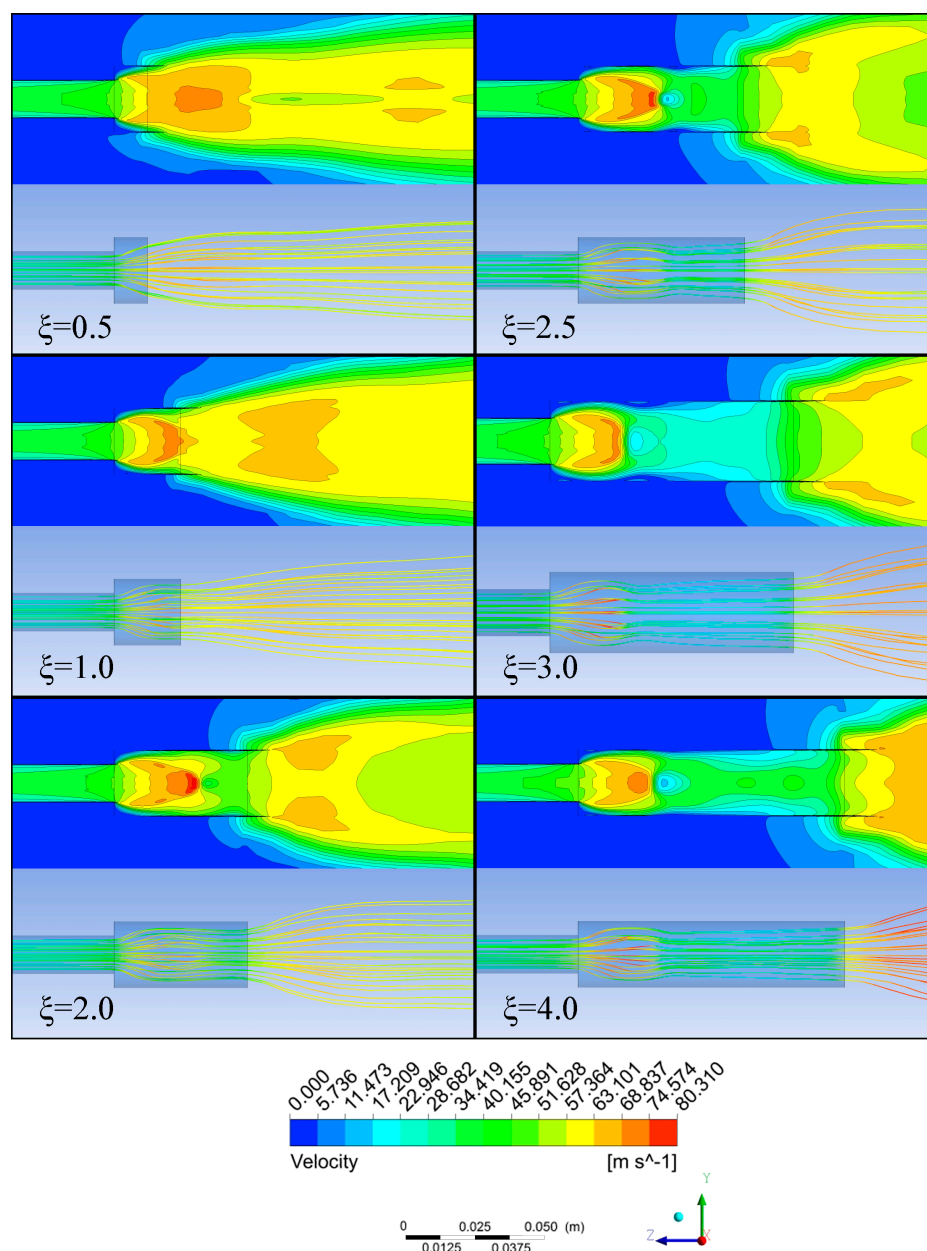


Figure 11. Section velocity distribution and 3D streamlines under different length–diameter ratios.

In order to facilitate the analysis of the velocity distribution characteristics during the flow process, as shown in Figure 12a, the variation curves of the velocity on the central axis towards the nozzle outlet direction under different length–diameter aspect ratios were plotted. It can be seen from the figure that the relative position relationship between the position where the maximum velocity on the central axis appeared and the nozzle outlet can also be clearly divided into two types, namely, when $\xi < 2$, the maximum velocity on the central axis inside the nozzle appeared on the outlet cross-section of the nozzle; however, when $\xi \geq 2$, it appeared inside the nozzle. Moreover, when $\xi < 2$, the velocity on the central axis inside the nozzle increased monotonically with the distance from the expansion position to the downstream, whereas when $\xi \geq 2$, as shown by dotted lines, the velocity on the central axis inside the nozzle showed obvious oscillation characteristics, which also should be a manifestation of the internal flow field in the nozzle transformed into the under-expanded flow structure.

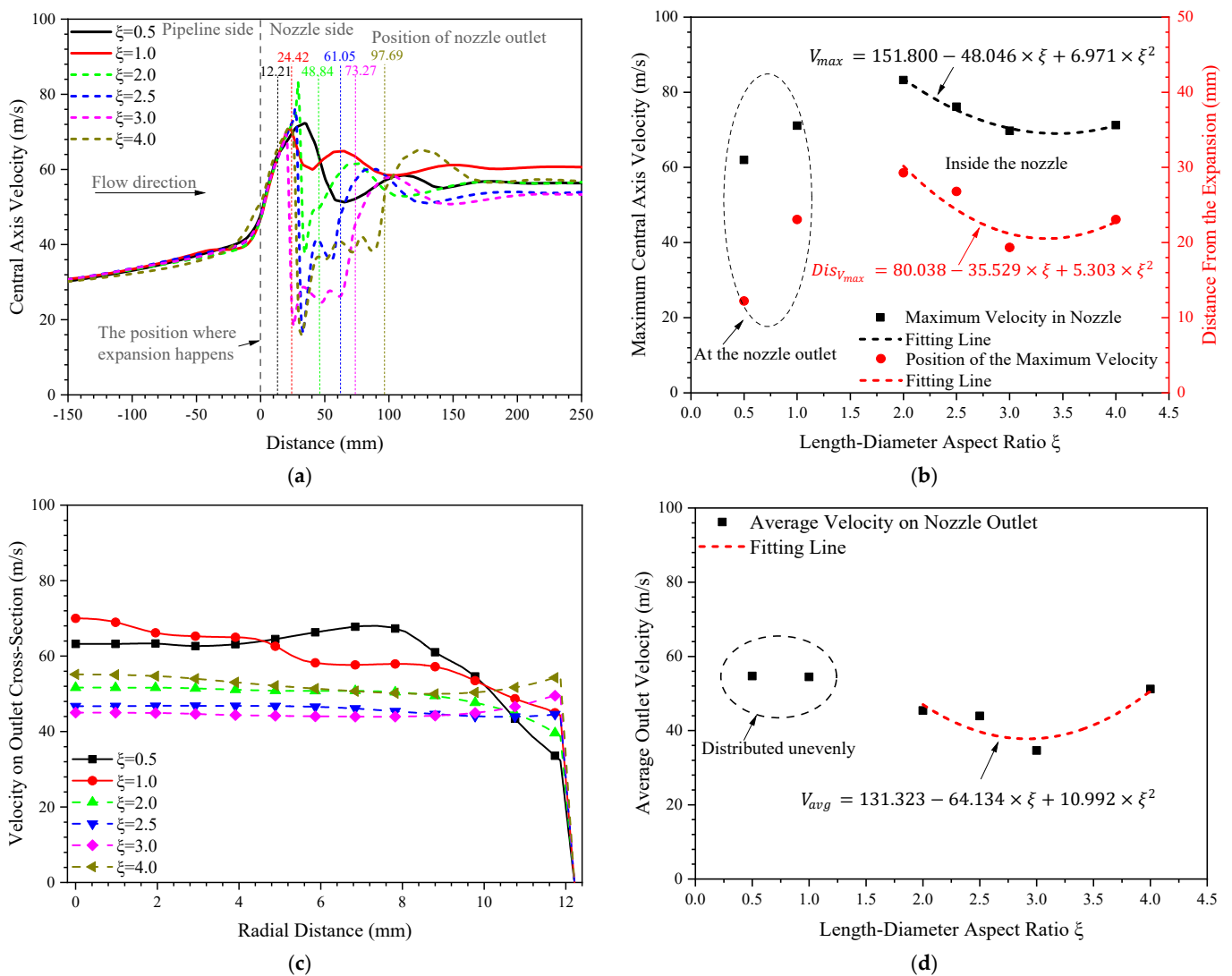


Figure 12. Variation of axial velocity under different length–diameter aspect ratios: (a) central axis velocity curves; (b) maximum velocity and distance; (c) velocity variation with the radius; (d) average velocity on the nozzle outlet cross-section.

Figure 12b shows the variations of the maximum velocity on the central axis in the nozzle (V_{max}) and the distance of the position where the maximum pressure appeared from the position where the area expansion occurred ($Dis_{V_{max}}$) vs. ξ . It can be seen from the figure that the variation of V_{max} and $Dis_{V_{max}}$ with ξ can also be clearly divided into two parts, namely, when $\xi < 2$, as shown by the dotted ellipse in the figure, the value of V_{max} was relatively small, and the value of $Dis_{V_{max}}$ was equal to the value of the nozzle expansion section length (L_2); when $\xi \geq 2$, with the increase of ξ , the values of V_{max} and $Dis_{V_{max}}$ both decreased first and then increased slightly. They can be fitted by quadratic polynomial functions, and the fitting results are shown in Equations (17) and (18).

$$V_{max} = 151.800 - 48.046 \times \xi + 6.971 \times \xi^2 \quad (17)$$

$$Dis_{V_{max}} = 80.038 - 35.529 \times \xi + 5.303 \times \xi^2 \quad (18)$$

where V_{max} represents the maximum velocity in the nozzle (m/s); $Dis_{V_{max}}$ denotes the distance of the position where the maximum velocity appears from the position where the area expansion happens (mm); and ξ represents the length–diameter aspect ratio of the nozzle.

In order to analyze the influence of ζ on the axial velocity at the nozzle outlet, as shown in Figure 12c, we plotted the variation of the axial velocity on the outlet cross-section of the nozzle with the radius against ζ . It can be seen from the figure that when $\zeta \geq 2$, the uniformity of the axial velocity distribution on the outlet cross-section was obviously improved compared with that in the case of $\zeta < 2$. This may have been due to the fact that the increase in the length of the expansion section was conducive to the full mixing and diffusion of the gaseous and liquid extinguishing agents in the expansion section.

Figure 12d shows the average axial velocity on the nozzle outlet cross-section (V_{avg}) vs. ζ . It can be seen from the figure that when $\zeta < 2$, V_{avg} was relatively large, and there was little difference between the two values, shown in the dotted ellipse in the figure corresponding to the cases of $\zeta = 0.5$ and $\zeta = 1.0$. This may have been due to the fact that the length of the expansion section was short, and the extinguishing agent had reached the nozzle outlet before it was rapidly vaporized in the expansion section of the nozzle. However, when $\zeta \geq 2$, with the continuous increase of ζ , V_{avg} decreased first and then increased, and the minimum value occurred under the condition of $\zeta = 3.0$.

Alongside the foregoing analysis, it can be speculated that this may be related to the change of the flow field structure in the nozzle. Moreover, with the increase of the length of expansion section, on the one hand, the flow resistance of the gas–liquid two-phase extinguishing agents will increase, and on the other hand, more extinguishing agents will inevitably vaporize during the flow process inside the nozzle. Therefore, V_{avg} presents the aforementioned non-monotonic variation trend. It can be fitted by a quadratic polynomial function, as shown in Equation (19).

$$V_{avg} = 131.323 - 64.134 \times \zeta + 10.992 \times \zeta^2 \tag{19}$$

where V_{avg} represents the average axial velocity on the cross-section of the nozzle outlet (m/s), and ζ denotes the length–diameter aspect ratio of the nozzle.

3.3. Effects of Wall Roughness on the Release Characteristics

3.3.1. Effects of Wall Roughness on the Pressure Characteristics

In order to facilitate the analysis of the pressure distribution characteristics during the flow process, as shown in Figure 13a, we plotted the variation curves of the pressure on the central axis of the pipeline and the nozzle under different wall roughnesses of the nozzle. It can be seen from the figure that the pressure on the central axis in the nozzle did not change significantly with the increase of the nozzle wall roughness.

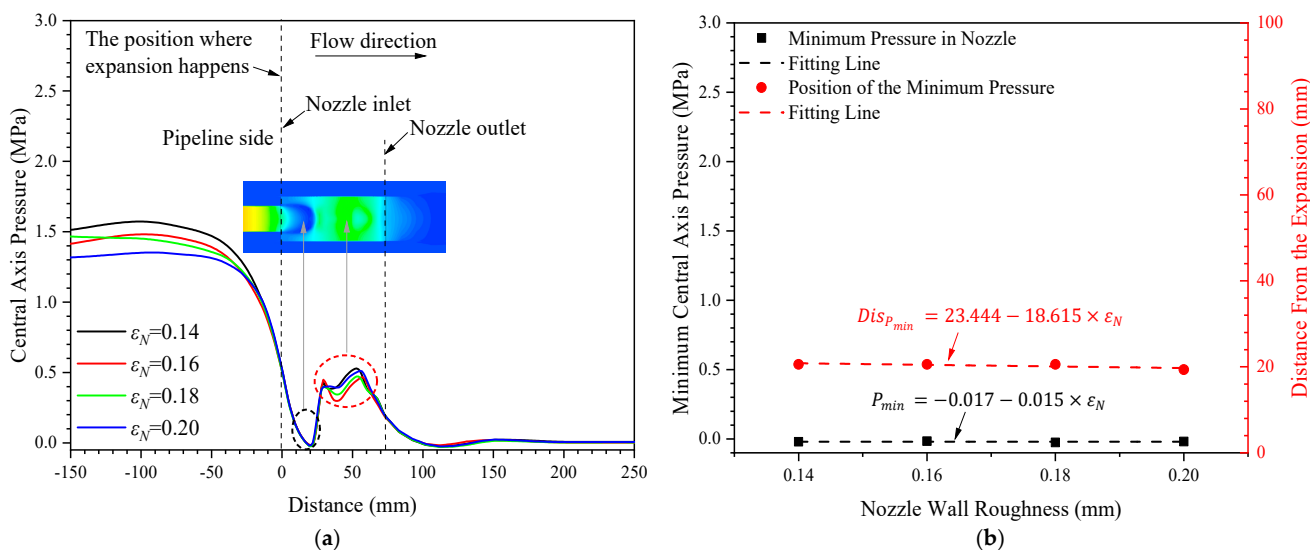


Figure 13. Cont.

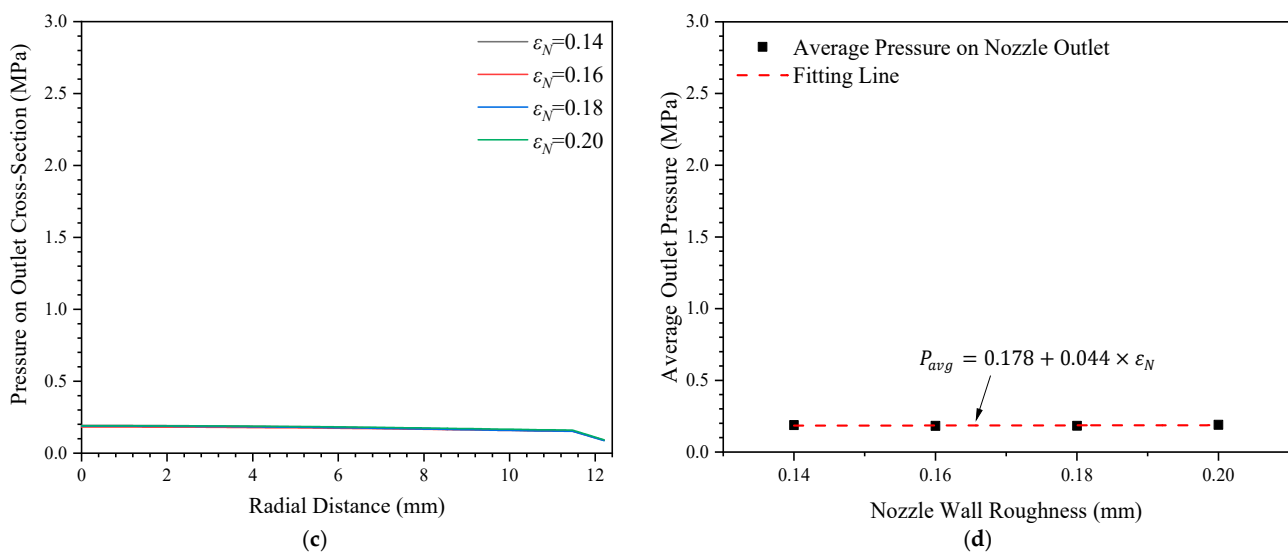


Figure 13. Variation of pressure under different wall roughness: (a) central axis pressure curves; (b) minimum pressure and distance; (c) pressure variation with the radius; (d) average pressure on the nozzle outlet cross-section.

Specifically, the pressure curves on the central axis in the low-pressure region (as shown by the black dotted ellipse in the figure) under different nozzle wall roughnesses were almost consistent, and the pressure on the central axis of the downstream region of the low-pressure zone in the nozzle (as shown by the red dotted ellipse in the figure) showed a slight non-monotonic change with the increase of the nozzle wall roughness. This may have been due to the fact that in the region where the sudden expansion occurred, the liquid extinguishing agent had not yet fully contacted with the nozzle wall, and therefore in the region near the nozzle inlet, the pressure did not change much with the increase of the nozzle wall roughness.

However, in the downstream region of the low-pressure zone, on the one hand, since the extinguishing agent made full contact with the wall, the increase of the wall roughness will inevitably increase the flow resistance and thus increase the pressure in the nozzle. On the other hand, the increase of the internal pressure will in turn slow down the gasification rate of the extinguishing agent, and therefore the pressure on the central axis presents the aforementioned non-monotonic slight change trend with the increase of the nozzle wall roughness.

Figure 13b shows the variations of the minimum pressure on the central axis in the nozzle (P_{min}) and the distance of the position where the minimum pressure appeared from the position where the area expansion occurred ($Dis_{P_{min}}$) vs. ε_N . It can be seen from the figure that P_{min} and $Dis_{P_{min}}$ had little change with the increase of ε_N . They can be fitted by linear functions, and the fitting results are shown in Equations (20) and (21).

$$P_{min} = -0.017 - 0.015 \times \varepsilon_N \quad (20)$$

$$Dis_{P_{min}} = 23.444 - 18.615 \times \varepsilon_N \quad (21)$$

where P_{min} represents the minimum pressure in the nozzle (Mpa); $Dis_{P_{min}}$ denotes the distance of the position where the minimum pressure appears from the position where the area expansion happens (mm); and ε_N represents the wall roughness of the nozzle (mm).

Figure 13c shows the variation curves of the pressure on the outlet cross-section of the nozzle with the radius under different conditions of ε_N . It can be seen from the figure that the pressure on the outlet cross-section did not change much with the radius, and the four pressure curves were almost consistent. This indicates that the increase of the nozzle wall roughness had little influence on the pressure on the outlet cross-section (P_{avg}) of the nozzle. In order to analyze the global influence of the wall roughness on the pressure on the nozzle outlet, we plotted the average pressure on the nozzle outlet cross-section against

ε_N , and the results are shown in Figure 13d. It can be seen from the figure that the change of P_{avg} with the increase of ε_N was also small. It can also be fitted by a linear function, as shown in Equation (22).

$$P_{avg} = 0.178 + 0.044 \times \varepsilon_N \quad (22)$$

where P_{avg} represents the average pressure on the cross-section of the nozzle outlet (MPa), and ε_N denotes the nozzle wall roughness (mm).

3.3.2. Effects of Wall Roughness on the Velocity Characteristics

Figure 14a shows the variation curves of the velocity on the central axis towards the nozzle outlet direction under different conditions of nozzle wall roughness (ε_N). It can be seen from the figure that the curves of the central axis velocity were almost consistent under the four different nozzle wall roughnesses, which indicates that the increase of ε_N had little influence on the central axis velocity in the nozzle.

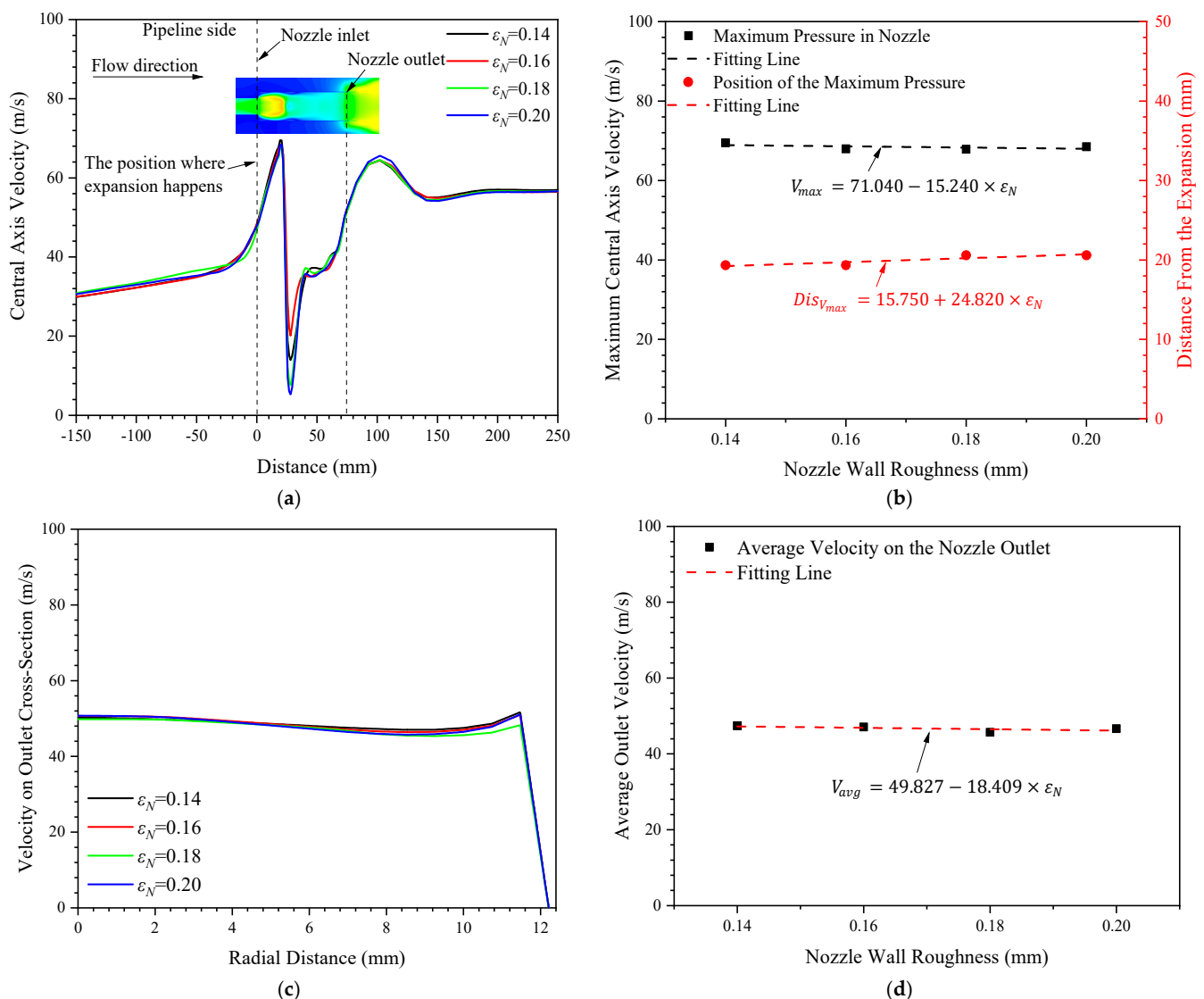


Figure 14. Variation of velocity under different wall roughness: (a) central axis velocity curves; (b) maximum velocity and distance; (c) velocity variation with the radius; (d) average velocity on the nozzle outlet cross-section.

In order to analyze the maximum velocity in the nozzle, as shown in Figure 14b, we plotted the variations of the maximum velocity on the central axis in the nozzle (V_{max}) and the distance of the position where the maximum pressure appeared from the position where the area expansion occurred ($Dis_{V_{max}}$) with ε_N . It can be seen from Figure 14b that

with the increase of ε_N , V_{max} decreased slightly, while $Dis_{V_{max}}$ increased slightly. This may have been due to the fact that the increase of ε_N increased the flow resistance in the nozzle, which made the maximum velocity decrease slightly and made the extinguishing agent need to flow relatively far to reach the maximum velocity. Both V_{max} and $Dis_{V_{max}}$ can be fitted by linear functions, and the fitting results are shown in Equations (23) and (24).

$$V_{max} = 71.040 - 15.240 \times \varepsilon_N \quad (23)$$

$$Dis_{V_{max}} = 15.750 + 24.820 \times \varepsilon_N \quad (24)$$

where V_{max} represents the maximum velocity in the nozzle (m/s); $Dis_{V_{max}}$ denotes the distance of the position where the maximum velocity appears from the position where the area expansion happens (mm); and ε_N represents the nozzle wall roughness (mm).

In order to analyze the influence of ε_N on the axial velocity at the nozzle outlet, as shown in Figure 14c, we plotted the variation of the axial velocity on the outlet cross-section of the nozzle with the outlet radius against ε_N . It can be seen from Figure 14c that the overall variation of the axial velocity on the outlet cross-section with ε_N was small. This indicates that ε_N had little influence on the axial velocity on the outlet cross-section.

Figure 14d shows the average axial velocity on the nozzle outlet cross-section (V_{avg}) vs. ε_N . It can be seen from the figure that within the value range of ε_N in this study, the changes of V_{avg} were very slight, and V_{avg} generally showed a slow decrease trend with the increase of ε_N . It can be fitted by a linear function, as shown in Equation (25).

$$V_{avg} = 49.827 - 18.409 \times \varepsilon_N \quad (25)$$

where V_{avg} represents the average axial velocity on the cross-section of the nozzle outlet (m/s), and ε_N denotes the nozzle wall roughness (mm).

4. Conclusions

A numerical simulation model of gas–liquid two-phase flow for the release characteristics of the straight sudden expansion nozzle was established in this work, which can provide guidance to the design of the release device of the aircraft-fixed gas fire-extinguishing system. On this basis, the influences of the outlet–inlet area ratio, length–diameter aspect ratio, and nozzle wall roughness on the pressure and velocity distribution characteristics inside the nozzle were studied. The major results and conclusions are summarized as follows:

- (1) The outlet–inlet area ratio δ had a significant effect on the release and flow characteristics of the straight sudden expansion gas extinguishing nozzle. With the increase of δ , the average pressure on the outlet cross-section of the nozzle decreased monotonically, while the average axial velocity on the outlet increased approximately linearly. In addition, with the increase of δ , the flow structure inside the nozzle can be divided into two stages. When $\delta \leq 1.5$, the distribution of pressure and velocity field in the nozzle was similar to those in the upstream pipeline, and the minimum pressure in the nozzle appeared at the outlet cross-section and the maximum velocity appeared much closer to the inlet of the nozzle. However, when $\delta > 1.5$, the flow structure in the nozzle changed into an obvious under-expanded flow structure, and with the increase of δ , the minimum pressure in the nozzle decreased gradually while the maximum axial velocity in the nozzle increased slightly, and the distance between the positions where the minimum pressure and the maximum velocity appeared in the nozzle and the position where sudden expansion occurred both increased gradually.
- (2) The length–diameter aspect ratio ζ also had a particularly significant impact on the release and flow characteristics of the straight sudden expansion gas extinguishing nozzle. When $\zeta < 2$, since the extinguishing agent had not sufficiently turbulently mixed in the expansion section before it reached the nozzle, both the minimum pressure on the central axis and the maximum axial velocity in the nozzle appeared on the nozzle outlet cross-section, and the pressure and velocity distribution on the

outlet were very uneven. When $\zeta \geq 2$, the uniformity of the pressure and velocity distribution on the nozzle outlet was significantly improved. Moreover, with the increase of ζ , the average pressure on the outlet increased first and then decreased, while the average axial velocity on the outlet decreased first and then increased. The results show that the optimal value of ζ should be about 3.0.

- (3) The nozzle wall roughness ε_N had a weak influence on the release and flow characteristics of the straight sudden expansion gas extinguishing nozzle. In the range of roughness from 0.14 to 0.20 mm studied in this paper, both the pressure and axial velocity in the nozzle did not change much with ε_N . With the increase of ε_N , the average pressure on the nozzle outlet increased slightly, while the average axial velocity on the nozzle outlet decreased slightly. This indicates that an increase in the wall roughness may reduce the release rate of the extinguishing agent to some extent.

Author Contributions: Conceptualization, Q.L.; methodology, J.L., X.H. and Y.C.; validation, Q.L. and R.C.; resources, Q.L., X.H. and Y.C.; data curation, J.L. and Q.L.; writing—original draft preparation, Q.L.; writing—review and editing, X.Z. and R.C.; visualization, Y.Z. and Q.L.; supervision, Q.L.; project administration, Q.L.; funding acquisition, R.C. and Q.L. All authors have read and agreed to the published version of the manuscript.

Funding: This research was funded by the China Postdoctoral Science Foundation (no. 2020M680069) and Jiangsu Planned Projects for Postdoctoral Research Funds (no. 2020Z414).

Institutional Review Board Statement: Not applicable.

Informed Consent Statement: Not applicable.

Data Availability Statement: The data will be made available on request from the corresponding author.

Conflicts of Interest: The authors declare no conflict of interest.

References

1. Hariram, S.S. *Fire Protection on Airplanes*; SAE International: Warrendale, PA, USA, 2005. [CrossRef]
2. Kurokawa, F.Y.; De Andrade, C.R.; Zaparoli, E.L. Modeling of aircraft fire suppression system by the lumped parameter approach. *Aircr. Eng. Aerosp. Technol.* **2016**, *88*, 535–539. [CrossRef]
3. Kim, J.; Baek, B.; Lee, J. Numerical analysis of flow characteristics of fire extinguishing agents in aircraft fire extinguishing systems. *J. Mech. Sci. Technol.* **2009**, *23*, 1877–1884. [CrossRef]
4. Payri, R.; Gimeno, J.; Martí-Aldaraví, P.; Carvallo, C. Parametrical study of the dispersion of an alternative fire suppression agent through a real-size extinguisher system nozzle under realistic aircraft cargo cabin conditions. *Process. Saf. Environ. Prot.* **2020**, *141*, 110–122. [CrossRef]
5. Dinesh, A.; Benson, C.M.; Holborn, P.G.; Sampath, S.; Xiong, Y. Performance evaluation of nitrogen for fire safety application in aircraft. *Reliab. Eng. Syst. Saf.* **2020**, *202*, 107044. [CrossRef]
6. Etzold, M.; Deswal, A.; Chen, L.; Durst, F. Break-up length of liquid jets produced by short nozzles. *Int. J. Multiph. Flow* **2018**, *99*, 397–407. [CrossRef]
7. Laurila, E.; Koivisto, S.; Kankkunen, A.; Saari, K.; Maakala, V.; Järvinen, M.; Vuorinen, V. Computational and experimental investigation of a swirl nozzle for viscous fluids. *Int. J. Multiph. Flow* **2020**, *128*, 103278. [CrossRef]
8. Pathan, K.A.; Dabeer, P.S.; Khan, S.A. Effect of Nozzle Pressure Ratio and Control Jets Location to Control Base Pressure in Suddenly Expanded Flows. *J. Appl. Fluid Mech.* **2019**, *12*, 1127–1135. [CrossRef]
9. Fathinia, F.; Khiadani, M.; Al-Abdeli, Y.M. Experimental and mathematical investigations of spray angle and droplet sizes of a flash evaporation desalination system. *Powder Technol.* **2019**, *355*, 542–551. [CrossRef]
10. Ji, H.; Li, Y.; Su, H.; Cheng, W.; Wu, X. Experimental Investigation on the Cooling and Inerting Effects of Liquid Nitrogen Injected into a Confined Space. *Symmetry* **2019**, *11*, 579. [CrossRef]
11. Halder, M.R.; Dash, S.K.; Som, S.K. A numerical and experimental investigation on the coefficients of discharge and the spray cone angle of a solid cone swirl nozzle. *Exp. Therm. Fluid Sci.* **2004**, *28*, 297–305. [CrossRef]
12. Sun, Y.; Alkhedhair, A.M.; Guan, Z.; Hooman, K. Numerical and experimental study on the spray characteristics of full-cone pressure swirl atomizers. *Energy* **2018**, *160*, 678–692. [CrossRef]
13. Xue, R.; Ruan, Y.; Liu, X.; Chen, L.; Liu, L.; Hou, Y. Numerical Study of the Effects of Injection Fluctuations on Liquid Nitrogen Spray Cooling. *Processes* **2019**, *7*, 564. [CrossRef]
14. Telega, J.; Szwaba, R.; Doerffer, P. Shock Waves Asymmetry in a Symmetric Nozzle. *Symmetry* **2019**, *11*, 1477. [CrossRef]
15. Yang, Y.; Karvounis, N.; Walther, J.H.; Ding, H.; Wen, C. Effect of area ratio of the primary nozzle on steam ejector performance considering nonequilibrium condensations. *Energy* **2021**, *237*, 121483. [CrossRef]

16. Lee, H.J.; Choi, H.; Jin, Y.-I.; Hwang, K.-Y.; Park, D.-C.; Min, S. Effect of nozzle inlet geometry in high temperature hydrocarbon liquid jets. *Int. J. Heat Fluid Flow* **2018**, *74*, 1–14. [[CrossRef](#)]
17. Ramesh, A.S.; Sekhar, S.J. Experimental and numerical investigations on the effect of suction chamber angle and nozzle exit position of a steam-jet ejector. *Energy* **2018**, *164*, 1097–1113. [[CrossRef](#)]
18. Fu, W.; Liu, Z.; Li, Y.; Wu, H.; Tang, Y. Numerical study for the influences of primary steam nozzle distance and mixing chamber throat diameter on steam ejector performance. *Int. J. Therm. Sci.* **2018**, *132*, 509–516. [[CrossRef](#)]
19. Zhang, R.; Liu, S.; Hu, X. Studies on the effects of structural parameters on jet characteristics of nozzles in lubricating aviation gears. *J. Aerosp. Power* **2016**, *31*, 2021–2028. [[CrossRef](#)]
20. Li, Z.-D.; Zhang, G.-Q.; Li, Z.; Zhang, Y.; Xu, W.-Y. Simulation of Gas Flow Field in Laval Nozzle and Straight Nozzle for Powder Metallurgy and Spray Forming. *J. Iron Steel Res. Int.* **2008**, *15*, 44–47. [[CrossRef](#)]
21. Cai, J.; Tsai, H.M.; Liu, F. Numerical simulation of vortical flows in the near field of jets from notched circular nozzles. *Comput. Fluids* **2010**, *39*, 539–552. [[CrossRef](#)]
22. Amini, G. Liquid flow in a simplex swirl nozzle. *Int. J. Multiph. Flow* **2016**, *79*, 225–235. [[CrossRef](#)]
23. Fu, W.; Li, Y.; Liu, Z.; Wu, H.; Wu, T. Numerical study for the influences of primary nozzle on steam ejector performance. *Appl. Therm. Eng.* **2016**, *106*, 1148–1156. [[CrossRef](#)]
24. Lee, H.J.; Choi, H.; Hwang, K.-Y.; Park, D.-C.; Min, S. Numerical study of choked cavitation in high temperature hydrocarbon liquid jets. *Int. J. Heat Fluid Flow* **2017**, *68*, 114–125. [[CrossRef](#)]
25. Lee, H.J.; Choi, H.; Park, D.-C. Hydraulic characteristics of high temperature hydrocarbon liquid jets with various orifice geometries. *Acta Astronaut.* **2018**, *152*, 657–666. [[CrossRef](#)]
26. Dong, J.; Hu, Q.; Yu, M.; Han, Z.; Cui, W.; Liang, D.; Ma, H.; Pan, X. Numerical investigation on the influence of mixing chamber length on steam ejector performance. *Appl. Therm. Eng.* **2020**, *174*, 115204. [[CrossRef](#)]
27. Shahzamanian, B.; Varga, S.; Soares, J.; Palmero-Marrero, A.; Oliveira, A. Performance evaluation of a variable geometry ejector applied in a multi-effect thermal vapor compression desalination system. *Appl. Therm. Eng.* **2021**, *195*, 117177. [[CrossRef](#)]
28. Yang, H.; Xu, Y.; Chen, Z.; Wang, W.; Aung, N.Z.; Li, S. Cavitation suppression in the nozzle-flapper valves of the aircraft hydraulic system using triangular nozzle exits. *Aerosp. Sci. Technol.* **2021**, *112*, 106598. [[CrossRef](#)]
29. Attou, A.; Giot, M.; Seynhaeve, J.-M. Modelling of steady-state two-phase bubbly flow through a sudden enlargement. *Int. J. Heat Mass Transf.* **1997**, *40*, 3375–3385. [[CrossRef](#)]
30. Roul, M.K.; Dash, S.K. Two-phase pressure drop caused by sudden flow area contraction/expansion in small circular pipes. *Int. J. Numer. Methods Fluids* **2010**, *66*, 1420–1446. [[CrossRef](#)]
31. Williamson, H.V. Halon 1301 flow in pipelines. *Fire Technol.* **1976**, *12*, 18–32. [[CrossRef](#)]
32. Fluent Corporation. *Fluent Help Documents*; Fluent Corporation: Canonsburg, PA, USA, 2015.
33. De Schepper, S.C.K.; Heynderickx, G.J.; Marin, G.B. Modeling the evaporation of a hydrocarbon feedstock in the convection section of a steam cracker. *Comput. Chem. Eng.* **2009**, *33*, 122–132. [[CrossRef](#)]
34. Fang, C.; David, M.; Rogacs, A.; Goodson, K. Volume of fluid simulation of boiling two-phase flow in a vapor-venting microchannel. *Front. Heat Mass Transf.* **2010**, *1*, 013002. [[CrossRef](#)]
35. Moen, A.; Mauri, L.; Narasimhamurthy, V.D. Comparison of k- ϵ models in gaseous release and dispersion simulations using the CFD code FLACS. *Process. Saf. Environ. Prot.* **2019**, *130*, 306–316. [[CrossRef](#)]
36. Li, Z. *Improvement of Waterjet and Abrasive Waterjet Nozzle*; New Jersey Institute of Technology: Newark, NJ, USA, 1994.
37. Zolfagharnasab, M.H.; Salimi, M.; Aghanajafi, C. Application of non-pressure-based coupled procedures for the solution of heat and mass transfer for the incompressible fluid flow phenomenon. *Int. J. Heat Mass Transf.* **2021**, *181*, 121851. [[CrossRef](#)]
38. Lin, Y.-H.; Li, X.-C. The Investigation of a Sliding Mesh Model for Hydrodynamic Analysis of a SUBOFF Model in Turbulent Flow Fields. *J. Mar. Sci. Eng.* **2020**, *8*, 744. [[CrossRef](#)]
39. Shukla, S.K.; Shukla, P.; Ghosh, P. Evaluation of numerical schemes using different simulation methods for the continuous phase modeling of cyclone separators. *Adv. Powder Technol.* **2011**, *22*, 209–219. [[CrossRef](#)]
40. Chen, F.; Yu, H.; Sun, Z.; Guo, Y. Determination of Inner Wall Roughness of Pipeline. *Oil Gas Transp. Storage* **2007**, *25*, 8–10.
41. Zhong, Q.; Chen, Q.; Wang, J.; Qu, H.; Ma, W.; Zhu, T.; Zhang, S. *Chemical Engineering Principles*, 4th ed.; National Defense Industry Press: Beijing, China, 2019; pp. 32–33.
42. Cafiero, G.; Ceglia, G.; Discetti, S.; Ianiro, A.; Astarita, T.; Cardone, G. On the three-dimensional precessing jet flow past a sudden expansion. *Exp. Fluids* **2014**, *55*, 1677. [[CrossRef](#)]